NACA TN 4021

NATIONAL ADVISORY COMMITTEE FOR AERONAUTICS

TECHNICAL NOTE 4021

NONUNIFORMITIES IN SHOCK-TUBE FLOW DUE TO UNSTEADY-BOUNDARY-LAYER ACTION

By Harold Mirels and W. H. Braun

Lewis Flight Propulsion Laboratory
Cleveland, Ohio

Washington
May 1957

4286

CF-1

NATIONAL ADVISORY COMMITTEE FOR AERONAUTICS

TECHNICAL NOTE 4021

NONUNIFORMITIES IN SHOCK-TUBE FLOW DUE TO UNSTEADY-BOUNDARY-LAYER ACTION

By Harold Mirels and W. H. Braun

SUMMARY

The boundary layer along the walls of a shock tube induces pressure and velocity gradients within the core of potential flow. These nonuniformities are evaluated herein for shock tubes in which the boundary layer is thin relative to the tube diameter and is either wholly laminar or wholly turbulent. The hot gas region between the shock wave and the contact surface is considered. Both the axial distributions at any instant and the temporal distributions at any axial position within this region are found. Numerical computations are presented for an air-air shock tube.

INTRODUCTION

The analysis of reference 1 obtains the flow perturbations, due to unsteady-boundary-layer action, immediately behind the shock wave in a shock tube. In this report the method will be extended to find the flow perturbations in the entire region between the shock wave and the contact surface. These perturbations are of interest when experimental shock-tube data are analyzed. As in the previous work, the assumptions are made that the boundary-layer action is equivalent to a one-dimensional distribution of mass sources and that the expansion wave has zero thickness. Numerical results are obtained for an air-air shock tube for which the initial temperature throughout the tube is 520° R, the wall boundary layer is either wholly laminar or wholly turbulent, and the shock-tube wall remains at a temperature of 520° R. The spatial and temporal variations in the hot gas region are presented graphically.

A theoretical study of the perturbations in the hot gas region between the shock and the contact surface is reported in reference 2. The limitations of the method of reference 2 are discussed in reference 1. A comparison of some of the results of reference 2 with those of the present report is made in the body of this report. It might also be noted that the method of reference 2 is also applied in reference 3 to estimate the perturbations in the expansion fan of a shock tube.

4286

ANALYSIS

Perturbations

In the following analysis, familiarity with reference 1 is assumed. The region between the shock wave and the contact surface is considered. The perturbation at an arbitrary point in this region (point $d(x,t)$ in fig. 1) is found by summing the pressure impulses which arrive at that point from both the left and the right. This summation requires an integration along all those characteristics influencing point $d(x,t)$. The characteristic lines considered herein are indicated in figure 1. Expressions for these characteristic lines are given by the following equations in terms of ξ,τ. The equations for $u_s\tau - \xi$, included therein, will be useful in later developments in this report. (Symbols are defined in appendix A.)

Characteristic lines:

bd

$$\left.\begin{aligned} x - \xi &= (a_2 + u_2)(t - \tau) \\ u_s\tau - \xi &= (x - \xi)\frac{1 + M_2 - \frac{u_s}{a_2}}{1 + M_2} + u_s t - x \end{aligned}\right\} \qquad (1a)$$

ab

$$\left.\begin{aligned} \xi_b - \xi &= (a_3 + u_3)(\tau_b - \tau) \\ a_4\tau + \xi &= (\xi - \xi_a)\frac{1 + M_3 + a_{43}}{1 + M_3} \end{aligned}\right\} \qquad (1b)$$

bc

$$\left.\begin{aligned} \xi - \xi_b &= (a_2 - u_2)(\tau_b - \tau) \\ u_s\tau - \xi &= (\xi_c - \xi)\frac{1 - M_2 + \frac{u_s}{a_2}}{1 - M_2} \end{aligned}\right\} \qquad (1c)$$

$\overline{bd}$

$$\left.\begin{aligned} \xi_{\overline{d}} - \xi &= (a_2 + u_2)(\tau_{\overline{d}} - \tau) \\ u_s\tau - \xi &= (\xi_{\overline{d}} - \xi)\frac{1 + M_2 - \frac{u_s}{a_2}}{1 + M_2} \end{aligned}\right\} \qquad (1d)$$

$\overline{ab}$

$$\left.\begin{aligned} \xi_{\overline{b}} - \xi &= (a_3 + u_3)(\tau_{\overline{b}} - \tau) \\ a_4\tau + \xi &= (\xi - \xi_{\overline{a}}) \frac{1 + M_3 + a_{43}}{1 + M_3} \end{aligned}\right\} \tag{1e}$$

$\overline{bc}$

$$\left.\begin{aligned} \xi - \xi_{\overline{b}} &= (a_2 - u_2)(\tau_{\overline{b}} - \tau) \\ u_s\tau - \xi &= (\xi_{\overline{c}} - \xi) \frac{1 - M_2 + \frac{u_s}{a_2}}{1 - M_2} \end{aligned}\right\} \tag{1f}$$

$\overline{dd}$

$$\left.\begin{aligned} \xi - x &= (a_2 - u_2)(t - \tau) \\ u_s\tau - \xi &= (x - \xi) \frac{1 - M_2 + \frac{u_s}{a_2}}{1 - M_2} + u_s t - x \end{aligned}\right\} \tag{1g}$$

Following the method of reference 1, the contribution to the pressure perturbation at point d in region 2 (hot gas) from waves arriving from the left is

$$\Delta p^{+}_{2,d} = \frac{2\gamma_2 p_2}{a_2 d} \frac{1}{1 + M_2} \int_{\xi_b}^{x} v_2 \, d\xi + C \frac{2\gamma_2 p_2}{a_2 d} \frac{1}{1 - M_2} \int_{\xi_b}^{\xi_c} v_2 \, d\xi +$$

$$D \frac{2\gamma_3 p_3}{a_3 d} \frac{1}{1 + M_3} \int_{\xi_a}^{\xi_b} v_3 \, d\xi$$

$$\equiv I^{+}_{bd} + CI^{-}_{bc} + DI^{+}_{ab} \tag{2}$$

The integrand is, in each case, the vertical velocity at the edge of the boundary layer. Coefficients C and D are, respectively, the reflection coefficient and the transmission coefficient at the interface between regions 2 and 3. They are derived in reference 1, appendix C, and equal:

$$\left.\begin{aligned} C &= \frac{\gamma_{32}a_{23} - 1}{\gamma_{32}a_{23} + 1} \\ D &= \frac{2}{\gamma_{32}a_{23} + 1} \end{aligned}\right\} \tag{3}$$

4286

CF-1 back

The waves arriving at point d from the right contribute a pressure perturbation

$$\Delta p_{2,d}^{-} = \frac{2\gamma_2 p_2}{a_2 d} \frac{1}{1 - M_2} \int_x^{\xi_{\bar{d}}} v_2 \, d\xi + E \frac{2\gamma_2 p_2}{a_2 d} \frac{1}{1 + M_2} \int_{\xi_{\bar{b}}}^{\xi_{\bar{d}}} v_2 \, d\xi +$$

$$EC \frac{2\gamma_2 p_2}{a_2 d} \frac{1}{1 - M_2} \int_{\xi_{\bar{b}}}^{\xi_{\bar{c}}} v_2 \, d\xi + ED \frac{2\gamma_3 p_3}{a_3 d} \frac{1}{1 + M_3} \int_{\xi_{\bar{a}}}^{\xi_{\bar{b}}} v_3 \, d\xi$$

$$\equiv I_{\bar{d}\bar{d}}^{-} + E \, I_{\bar{b}\bar{d}}^{+} + EC \, I_{\bar{b}\bar{c}}^{-} + ED \, I_{\bar{a}\bar{b}}^{+} \tag{4}$$

The reflection coefficient E at the shock is defined in reference 1, appendix C, as

$$E = \frac{2\rho_{12} a_{12} \dfrac{M_s^3}{1 + M_s^2} - 1}{2\rho_{12} a_{12} \dfrac{M_s^3}{1 + M_s^2} + 1} \tag{5}$$

The contributions to $\Delta p_{2,d}^{+}$ and $\Delta p_{2,d}^{-}$ from waves reflected at points c and $\bar{c}$ are shown to be negligible in reference 1.

The limits of the integrals in equations (2) and (4) are the end points of the characteristic line segments (eqs. (1)). They may be evaluated in terms of the coordinates x,t at point d as follows:

a

$$\left.\begin{aligned} \xi_a &= \frac{a_{43}x - (1 + M_2)a_4 t}{1 + M_3 + a_{43}} \\ \tau_a &= \frac{(1 + M_2)t - \dfrac{x}{a_2}}{1 + M_3 + a_{43}} \end{aligned}\right\} \tag{6a}$$

4286

b

$$\left.\begin{aligned} \xi_b &= (1 + M_2)u_2t - M_2x \\ \tau_b &= (1 + M_2)t - \frac{x}{a_2} \end{aligned}\right\} \tag{6b}$$

c

$$\left.\begin{aligned} \xi_c &= \frac{(1 + M_2)u_st - \left(\frac{u_s}{a_2}\right)x}{1 - M_2 + \frac{u_s}{a_2}} \\ \tau_c &= \frac{(1 + M_2)t - \frac{x}{a_2}}{1 - M_2 + \frac{u_s}{a_2}} \end{aligned}\right\} \tag{6c}$$

$\overline{a}$

$$\left.\begin{aligned} \xi_{\overline{a}} &= \frac{-\frac{a_4}{u_3}}{1 + M_3 + a_{43}} \frac{1 + M_2 - \frac{u_s}{a_2}}{1 - M_2 + \frac{u_s}{a_2}} \left[(1 - M_2)u_2t + M_2x\right] \\ \tau_{\overline{a}} &= \frac{1}{1 + M_3 + a_{43}} \frac{1 + M_2 - \frac{u_s}{a_2}}{1 - M_2 + \frac{u_s}{a_2}} \left[(1 - M_2)t + \frac{x}{a_2}\right] \end{aligned}\right\} \tag{6d}$$

$\overline{b}$

$$\left.\begin{aligned} \xi_{\overline{b}} &= \frac{1 + M_2 - \frac{u_s}{a_2}}{1 - M_2 + \frac{u_s}{a_2}} \left[(1 - M_2)u_2t + M_2x\right] \\ \tau_{\overline{b}} &= \frac{1 + M_2 - \frac{u_s}{a_2}}{1 - M_2 + \frac{u_s}{a_2}} \left[(1 - M_2)t + \frac{x}{a_2}\right] \end{aligned}\right\} \tag{6e}$$

$$\left.\begin{aligned}
\overline{c} \qquad \xi_{\overline{c}} &= \frac{1 + M_2 - \dfrac{u_s}{a_2}}{\left(1 - M_2 + \dfrac{u_s}{a_2}\right)^2}\left[(1 - M_2)u_s t + \left(\frac{u_s}{a_2}\right)x\right] \\
\tau_{\overline{c}} &= \frac{1 + M_2 - \dfrac{u_s}{a_2}}{\left(1 - M_2 + \dfrac{u_s}{a_2}\right)^2}\left[(1 - M_2)t + \frac{x}{a_2}\right]
\end{aligned}\right\} \tag{6f}$$

$$\left.\begin{aligned}
\overline{d} \qquad \xi_{\overline{d}} &= \frac{(1 - M_2)u_s t + \left(\dfrac{u_s}{a_2}\right)x}{1 - M_2 + \dfrac{u_s}{a_2}} \\
\tau_{\overline{d}} &= \frac{(1 - M_2)t + \dfrac{x}{a_2}}{1 - M_2 + \dfrac{u_s}{a_2}}
\end{aligned}\right\} \tag{6g}$$

The vertical velocity at the edge of the boundary layer is expressed in reference 1, appendixes D and E, as

$$\left.\begin{aligned}
v_2 &= -L_2\left(\frac{\dfrac{u_2^2}{u_s}}{1 - \dfrac{u_2}{u_s}}\right)^{1-n_2}\left(\frac{\nu_2}{u_s\tau - \xi}\right)^{n_2} \qquad \text{(region 2)} \\
v_3 &= L_3\left(\frac{\dfrac{u_3^2}{a_4}}{1 + \dfrac{u_3}{a_4}}\right)^{1-n_3}\left(\frac{\nu_3}{a_4\tau + \xi}\right)^{n_3} \qquad \text{(region 3)}
\end{aligned}\right\} \tag{7}$$

The two coefficients L_2 and L_3 are evaluated in reference 1 for both wholly laminar and wholly turbulent boundary layers. The indices n_2 and n_3 are 1/2 for laminar boundary layers and 1/5 for turbulent boundary layers.

The use of equations (6) and (7) leads to the following values of the integrals in equation (2):

$$I_{bd}^{+} \equiv \frac{2\gamma_2 p_2}{a_2 d} \frac{1}{1 + M_2} \int_{\xi_b}^{x} v_2 \, d\xi$$

$$= \frac{2\gamma_2 p_2 L_2}{d(1 - n_2)} \frac{\left(\frac{\nu_2}{a_2}\right)^{n_2} \left(\frac{M_2^2}{\frac{u_s}{a_2} - M_2}\right)^{1-n_2}}{1 + M_2 - \frac{u_s}{a_2}} \left(\left(1 - \frac{x}{u_s t}\right)^{1-n_2} - \left\{\left(\frac{u_s}{a_2} - M_2\right)\left[(1 + M_2)\frac{a_2}{u_s} - \frac{x}{u_s t}\right]\right\}^{1-n_2}\right)(u_s t)^{1-n_2} \tag{8a}$$

$$I_{bc}^{-} \equiv \frac{2\gamma_2 p_2}{a_2 d} \frac{1}{1 - M_2} \int_{\xi_b}^{\xi_c} v_2 \, d\xi$$

$$= \frac{-2\gamma_2 p_2 L_2}{d(1 - n_2)} \frac{\left(\frac{\nu_2}{a_2}\right)^{n_2} (M_2^2)^{1-n_2}}{1 - M_2 + \frac{u_s}{a_2}} \left[(1 + M_2)\frac{a_2}{u_s} - \frac{x}{u_s t}\right]^{1-n_2} (u_s t)^{1-n_2} \tag{8b}$$

$$I_{d\bar{d}}^{-} \equiv \frac{2\gamma_2 p_2}{a_2 d} \frac{1}{1 - M_2} \int_{x}^{\xi_{\bar{d}}} v_2 \, d\xi$$

$$= \frac{2\gamma_2 p_2 L_2}{d(1 - n_2)} \frac{\left(\frac{\nu_2}{a_2}\right)^{n_2}}{1 - M_2 + \frac{u_s}{a_2}} \left(\frac{M_2^2}{\frac{u_s}{a_2} - M_2}\right)^{1-n_2} \left(1 - \frac{x}{u_s t}\right)^{1-n_2} (u_s t)^{1-n_2} \tag{8c}$$

$$I_{\bar{b}c}^{-} \equiv \frac{2\gamma_2 p_2}{a_2 d} \frac{1}{1 - M_2} \int_{\xi_{\bar{b}}}^{\xi_{\bar{c}}} v_2 \, d\xi$$

$$= \frac{-2\gamma_2 p_2 L_2}{d(1 - n_2)} \frac{\left(\frac{\nu_2}{a_2}\right)^{n_2} (M_2^2)^{1-n_2}}{1 - M_2 + \frac{u_s}{a_2}} \left(\frac{1 + M_2 - \frac{u_s}{a_2}}{1 - M_2 + \frac{u_s}{a_2}}\right)^{1-n_2} \left[(1 - M_2)\frac{a_2}{u_s} + \frac{x}{u_s t}\right]^{1-n_2} (u_s t)^{1-n_2} \tag{8d}$$

$$I^{+}_{\bar{b}\bar{d}} \equiv \frac{2\gamma_2 p_2}{a_2 d} \frac{1}{1 + M_2} \int_{\xi_{\bar{b}}}^{\xi_{\bar{d}}} v_2 \, d\xi$$

$$= \frac{-2\gamma_2 p_2 L_2}{d(1 - n_2)} \frac{\left(\frac{\nu_2}{a_2}\right)^{n_2} (M_2^2)^{1-n_2}}{1 + M_2 - \frac{u_s}{a_2}} \left(\frac{1 + M_2 - \frac{u_s}{a_2}}{1 - M_2 + \frac{u_s}{a_2}}\right)^{1-n_2} \left[(1 - M_2) \frac{a_2}{u_s} + \frac{x}{u_s t}\right]^{1-n_2} (u_s t)^{1-n_2} \tag{8e}$$

$$I^{+}_{ab} \equiv \frac{2\gamma_3 p_3}{a_3 d} \frac{1}{1 + M_3} \int_{\xi_a}^{\xi_b} v_3 \, d\xi$$

$$= \frac{2\gamma_3 p_3 L_3}{d(1 - n_3)} \frac{\left(\frac{\nu_3}{a_3}\right)^{n_3} (M_2^2)^{1-n_3} (a_{23})^{1-n_3}}{1 + M_3 + a_{43}} \left[(1 + M_2) \frac{a_2}{u_s} - \frac{x}{u_s t}\right]^{1-n_3} (u_s t)^{1-n_3} \tag{8f}$$

$$I^{+}_{\bar{a}\bar{b}} \equiv \frac{2\gamma_3 p_3}{a_3 d} \frac{1}{1 + M_3} \int_{\xi_{\bar{a}}}^{\xi_{\bar{b}}} v_3 \, d\xi$$

$$= \frac{2\gamma_3 p_3 L_3}{d(1 - n_3)} \frac{\left(\frac{\nu_3}{a_3}\right)^{n_3} (M_2^2)^{1-n_3} (a_{23})^{1-n_3}}{1 + M_3 + a_{43}} \left(\frac{1 + M_2 - \frac{u_s}{a_2}}{1 - M_2 + \frac{u_s}{a_2}}\right)^{1-n_3} \times$$

$$\left[(1 - M_2) \frac{a_2}{u_s} + \frac{x}{u_s t}\right]^{1-n_3} (u_s t)^{1-n_3} \tag{8g}$$

Under the assumptions that the boundary layer is wholly laminar or wholly turbulent ($n_2 = n_3 \equiv n$), the two pressure disturbances become

$$-1\,\frac{\Delta p_{2,d}^{+}}{p_2}\left(\frac{d}{u_s t}\right)^{1-n}\left(\frac{a_2 d}{\nu_2}\right)^{n}\frac{1-n}{2\gamma_2 L_2 (M_2^2)^{1-n}}$$

$$=\left(\frac{1}{1+M_2-\frac{u_s}{a_2}}+\frac{C}{1-M_2+\frac{u_s}{a_2}}-\frac{D\gamma_{32}L_{32}(\nu_{32})^{n}a_{23}}{1+M_3+a_{43}}\right)\left[(1+M_2)\frac{a_2}{u_s}-\frac{x}{u_s t}\right]^{1-n}-$$

$$\frac{1}{1+M_2-\frac{u_s}{a_2}}\left(\frac{1-\frac{x}{u_s t}}{\frac{u_s}{a_2}-M_2}\right)^{1-n} \tag{9a}$$

and

$$-1\,\frac{\Delta p_{2,d}^{-}}{p_2}\left(\frac{d}{u_s t}\right)^{1-n}\left(\frac{a_2 d}{\nu_2}\right)^{n}\frac{1-n}{2\gamma_2 L_2 (M_2^2)^{1-n}}=\frac{1}{1-M_2+\frac{u_s}{a_2}}\left(\frac{1-\frac{x}{u_s t}}{\frac{u_s}{a_2}-M_2}\right)^{1-n}+$$

$$E\left[\frac{1}{1+M_2-\frac{u_s}{a_2}}+\frac{C}{1-M_2+\frac{u_s}{a_2}}-\frac{D\gamma_{32}L_{32}(\nu_{32})^{n}a_{23}}{1+M_3+a_{43}}\right]\times$$

$$\left(\frac{1+M_2-\frac{u_s}{a_2}}{1-M_2+\frac{u_s}{a_2}}\right)^{1-n}\left[(1-M_2)\frac{a_2}{u_s}+\frac{x}{u_s t}\right]^{1-n} \tag{9b}$$

The complete pressure and velocity perturbations at point d are obtained from equation (9) according to

$$\Delta p_{2,d}=\Delta p_{2,d}^{+}+\Delta p_{2,d}^{-} \tag{10a}$$

$$\Delta u_{2,d}=\frac{1}{\rho_2 a_2}\left(\Delta p_{2,d}^{+}-\Delta p_{2,d}^{-}\right) \tag{10b}$$

4286

CF-2

Other perturbation quantities, such as temperature and density, can be found by the methods indicated in appendix B.

The axial distributions of the perturbations $\Delta p_{2,d}$ and $\Delta u_{2,d}$ at any instant of time are presented in figures 2 and 3 for several nominal shock numbers. An air-air shock tube with $T_1 = T_4 = 520^\circ$ R and wholly laminar or wholly turbulent boundary layers is considered. The wall temperature is assumed to remain constant at 520° R at all times. The ratio of specific heats γ and the Prandtl number were taken as 1.4 and 0.70, respectively. In each case the curve is normalized to the value $\Delta p_{2,o}$ (or $\Delta u_{2,o}$), which is the value of the perturbation immediately behind the shock wave at the instant of time under consideration. In using the plots of $\Delta p_{2,d}/\Delta p_{2,o}$, for example, the numerical value of $\Delta p_{2,o}$ may be obtained from equations (9) and (10a) evaluated at $x = u_s t$. A nondimensional plot of $\Delta p_{2,o}$ is given in reference 1 for an air-air shock tube and is reproduced here for convenience in figure 4. If an experimental observation of shock attenuation is made, $\Delta p_{2,o}$ can be determined directly from the experimental data (see, e.g., appendix B). Then figure 2 should yield accurate estimates of the axial variation of pressure between the shock and the contact surface at the fixed instant of time.

If equations (9a) and (9b) are multiplied by $(u_s t/x)^{1-n}$, they are brought into a form which gives the variation, with time, of the perturbations at a fixed axial station x (appendix B). This form is of interest when aerodynamic measurements are made at a fixed station in the shock tube. Numerical results are presented in figures 5 and 6 (for the air-air shock tube described in connection with figs. 2 and 3). The abscissa is the dimensionless time measured from the passage of the shock past the fixed station under consideration. The curves terminate at that time at which the contact surface passes the station. In figures 5 and 6, $\Delta p_{2,o}$ is the pressure perturbation directly behind the shock at the instant it passed the fixed station being considered. The numerical value of $\Delta p_{2,o}$ can again be determined by the methods described in appendix B.

Typical results of the present analysis are compared with those of reference 2 in figure 7. The temporal variation of pressure at a fixed station in an air-air shock tube is shown therein. The temperatures are $T_1 = T_4 = 520^\circ$ R; the axial position is 8 feet and the hydraulic diameter $d = 1/7$. The solid curves are based on equations (9). The dashed curves are from figure 8 of reference 2. It is seen that, for the range of Mach numbers considered, the method of reference 2 predicts a greater increment of the perturbation pressure in the hot gas than does the present method. For example, consider conditions at the contact surface

4286

for $p_{21} = 3.4$. The ratio $\Delta p_{2,d}/\Delta p_{2,o}$ equals -0.2 by the method of reference 2 and equals 0.2 by the present method. This represents a discrepancy of about 40 percent in the perturbation quantity $\Delta p_{2,d}/\Delta p_{2,o}$. The limitations of the method of reference 2 are discussed in reference 1.

Weak Shocks

If the same gas is used in regions 1 and 4 ($\gamma_1 = \gamma_4$) at the same initial temperature ($T_1 = T_4$), and if the boundary layers are wholly turbulent or wholly laminar ($n_2 = n_3$), then, for weak shocks ($M_s \approx 1$, $M_2 \ll 1$) the pressure and velocity perturbations may be found in terms of the single parameter M_2.

By using the relation

$$\frac{p_2}{p_1} = 1 + \gamma M_2 + O(M_2^2)$$

which may be obtained from the ideal shock-tube relations (as given, e.g., in appendix G of ref. 1), the transmission and reflection coefficients are found to be

$$C = \frac{\gamma - 1}{2} M_2 + O(M_2^2)$$

$$D = 1 - \frac{\gamma - 1}{2} M_2 + O(M_2^2)$$

$$E = O(M_2^2)$$

Also,

$$1 + M_2 - \frac{u_s}{a_2} = \frac{\gamma + 1}{4} M_2 + O(M_2^2)$$

$$L_{32} = \nu_{32} = a_{32} = 1 + O(M_2)$$

4286

CF-2 back

By neglecting higher-order terms in M_2, equations (9a) and (9b) become, respectively,

$$\left(\frac{d}{u_s t}\right)^{1-n}\left(\frac{a_2 d}{\nu_2}\right)^{n}\frac{1-n}{2\gamma_2 L_2 (M_2^2)^{1-n}}\frac{\Delta p_{2,d}^{+}}{p_2}$$

$$= \frac{4}{(\gamma+1)M_2}\left[\left(\frac{1-\frac{x}{u_s t}}{1-\frac{\gamma+1}{4}M_2}\right)^{1-n} - \left(1-\frac{\gamma+1}{8}M_2\right)\left(1+\frac{\gamma+1}{4}M_2-\frac{x}{u_s t}\right)^{1-n}\right] \tag{11a}$$

$$\left(\frac{d}{u_s t}\right)^{1-n}\left(\frac{a_2 d}{\nu_2}\right)^{n}\frac{1-n}{2\gamma_2 L_2 (M_2^2)^{1-n}}\frac{\Delta p_{2,d}^{-}}{p_2} = -\frac{1}{2}\left(\frac{1-\frac{x}{u_s t}}{1-\frac{\gamma+1}{4}M_2}\right)^{1-n} \tag{11b}$$

valid for $M_2 < x/u_s t < 1$. (The point $x/u_s t = M_2$ corresponds to the contact surface.) Equations (11) follow from equations (9) by neglecting the term containing C in equation (9a) and the terms containing E in equation (9b). The pressure and velocity perturbations in region 2 (eqs. (10a) and (b), respectively) are now found to be

$$\frac{\Delta p_{2,d}}{\Delta p_{2,o}} = \left[\frac{4}{(\gamma+1)M_2}\right]^{1-n}\left[\left(1+\frac{\gamma+1}{4}M_2-\frac{x}{u_s t}\right)^{1-n} - \left(\frac{1-\frac{x}{u_s t}}{1-\frac{\gamma+1}{4}M_2}\right)^{1-n}\right] \tag{12a}$$

$$\frac{\Delta u_{2,d}}{\Delta u_{2,o}} = \frac{\left(1-\frac{\gamma+1}{8}M_2\right)\left(1+\frac{\gamma+1}{4}M_2-\frac{x}{u_s t}\right)^{1-n} - \left(1+\frac{\gamma+1}{8}M_2\right)\left(\frac{1-\frac{x}{u_s t}}{1-\frac{\gamma+1}{4}M_2}\right)^{1-n}}{\left(1-\frac{\gamma+1}{8}M_2\right)\left(\frac{\gamma+1}{4}M_2\right)^{1-n}} \tag{12b}$$

The limiting forms (12a) and (12b) are shown in figures 8 and 9, respectively, for three values of M_2. The accuracy of the limiting forms is indicated by comparison with the dashed curves, which were obtained from equations (9) and (10) for $M_2 = 0.2$ ($M_s = 1.1328$). The corresponding time plots are shown in figures 10 and 11. They are obtained as the products of equations (12) and $(u_s t/x)^{1-n}$.

DISCUSSION OF RESULTS

The numerical results of the present analysis are presented in graphic form in figures 2 to 11. The normalized ratios $\Delta p_{2,d}/\Delta p_{2,o}$ and $\Delta u_{2,d}/\Delta u_{2,o}$ are used therein. It should be kept in mind that $\Delta p_{2,o}$ and $\Delta u_{2,o}$ are negative in all cases so that when these normalized ratios are positive or negative, the numerator is negative or positive, respectively. The ratios $\Delta p_{2,d}/\Delta p_{2,o}$ and $\Delta u_{2,d}/\Delta u_{2,o}$ are less when variations with x at a fixed t are considered than when variations with t at a fixed x (except at $x/u_s t = 1$) are considered, since $\Delta p_{2,o}$ and $\Delta u_{2,o}$ are larger for the former than for the latter (see sketch). The results for wholly laminar boundary layers exhibit the same trends as those for wholly turbulent boundary layers, although the individual perturbations are less for the laminar case (ref. 1). Hence, only the trends of the turbulent boundary-layer results will be discussed herein.

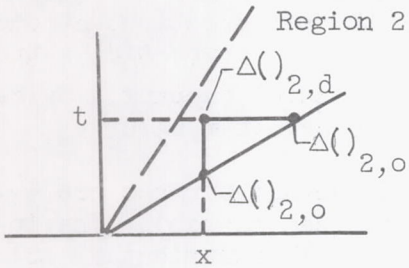

For weak shocks the ratio $\Delta p_{2,d}/\Delta p_{2,o}$ varies from 1 at the shock to nearly zero at the contact surface (figs. 8(b) and 10(b)). Thus, the pressure near the contact surface remains nearly at the ideal (i.e., no-attenuation) value. The ratio $\Delta u_{2,d}/\Delta u_{2,o}$ varies from 1 at the shock to a substantial negative value at the contact surface (figs. 9(b) and 11(b)). Thus the velocity perturbation at the contact surface is positive and the contact surface "speeds up" because of the wall boundary layer. This is observed experimentally in reference 4.

With increases in shock strength, the value of $\Delta p_{2,d}/\Delta p_{2,o}$ at the contact surface also increases (figs. 2(b) and 5(b)) so that a considerable pressure decrement exists at the contact surface. For strong shocks ($M_s = O(6)$) the pressure perturbation at the contact surface is of the same order of magnitude as that behind the shock so that the pressure is fairly uniform in region 2. This result is in qualitative agreement with the unpublished experimental measurements of J. J. Jones of the Langley laboratory, in which a relatively constant pressure region directly behind the shock is noted. With increase of M_s, the value of $\Delta u_{2,d}/\Delta u_{2,o}$ at the contact surface ultimately increases to a value of about 0 for $M_s \approx 6$ (figs. 3(b) and 6(b)). Thus for $M_s \approx 6$ the contact surface moves at approximately the ideal value. However, since the shock speed is lower than ideal, due to attenuation, the speed of the contact surface relative to the shock is greater than that predicted by ideal shock-tube

theory. This effect tends to reduce the available test time when experiments are conducted at a fixed station in a shock tube. Moreover, this results in a substantial variation of velocity in region 2 despite the fact that the pressure variation is relatively small.

The previously noted results can be explained on the following physical grounds. The boundary layer in region 3 generates longitudinal compression waves while that in region 2 generates expansion waves (ref. 1). The net effect of these waves is to attenuate the shock as described in reference 1. The shock attenuation defines the perturbations at one limit ($x/u_s t \approx 1$) of region 2. The variation of fluid properties between the shock and the contact surface can then be estimated (approx.) by consideration of conditions near the contact surface ($x/u_s t \approx u_2/u_s$). 4286

For weak shocks the perturbations near the contact surface are mainly due to the characteristic lines ab and $d\bar{d}$ (see sketch). The integration along line ab contributes, at point d, a compression wave moving in the $+x$-direction. The integration along line $d\bar{d}$ contributes an expansion wave moving in the -x-direction. For an air-air shock tube with small initial pressure ratio, these pressure waves are approximately of equal and opposite strength so that the pressure perturbations cancel each other (eq. (10a)) while the corresponding velocity perturbations are additive (eq. (10b)). Thus for weak shocks the pressure perturbation is essentially zero at the contact surface while the velocity perturbation has a substantial positive value. Other perturbation quantities can be readily found by using appendix B.

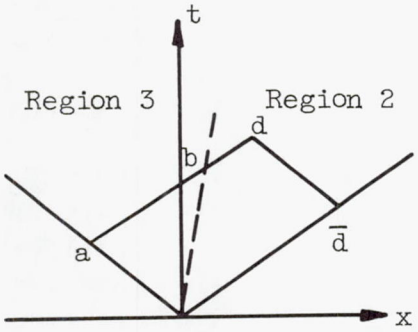

Now, consider the case of an air-air shock tube with a very high initial pressure ratio so that the shock strength is large. It can be shown that region 3 (i.e., characteristic line ab) makes only a small contribution to the perturbations at points near the contact surface. This is primarily due to the fact that the transmission coefficient D at point b (i.e., $D \equiv \Delta p^+_{2,b}/\Delta p^+_{3,b}$ is the ratio of the wave transmitted into region 2 to the incident wave arriving from region 3) approaches zero for the strong-shock case.

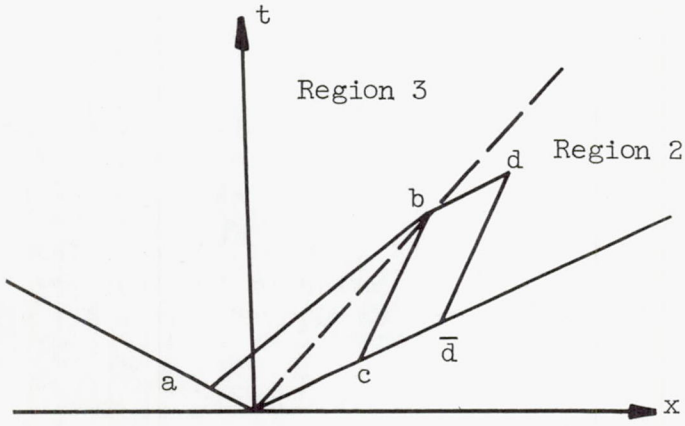

Thus the major contribution to the perturbations is due to characteristic lines $d\bar{d}$ and cb. The integrations of v_2 along lines $d\bar{d}$ and cb are very nearly equal when point d is near the contact surface. However, the contribution of line cb to point d is found by multiplying the integral along line cb by the reflection coefficient C (i.e., $C \equiv \Delta p_{2,b}^{+}/\Delta p_{2,b}^{-}$ is the ratio of the reflected to the incident wave, in region 2, at point b). But C approaches 1 for strong shocks so that the pressure perturbation at point d, due to line cb, is very nearly equal to that due to line $d\bar{d}$. However, since the contribution of line cb is a wave moving in the +x-direction (due to reflection at point b) while line $d\bar{d}$ contributes an approximately equal pressure wave moving in the -x-direction, the pressures are additive, but the resulting velocity perturbation is nearly zero. As a result the pressure decrement at the contact surface is of the same order as that behind the shock, but the velocity of the contact surface remains at essentially the ideal value. (The latter result could also be deduced by noting that the acoustic impedance ratio $\rho_3 a_3/\rho_2 a_2 = \gamma_3 a_2/\gamma_2 a_3$ is very high so that the contact surface tends to be a constant-velocity interface and at the pressure imposed by region 2.)

4286

The perturbations at a fixed station x for the case of a strong shock is discussed further in appendix B. It is noted therein that, during the time interval between passage of the shock and passage of the contact surface, $\Delta p_{2,d}/\Delta p_{2,o}$ remains at about 1, $\Delta u_{2,d}/\Delta u_{2,o}$ varies from 1 to 0, $\frac{\Delta\rho_{2,d}}{\rho_2}\frac{p_2}{\Delta p_{2,o}}$ varies from 0 to $\frac{1}{\gamma_1}$, $\frac{\Delta T_{2,d}}{T_2}\frac{p_2}{\Delta p_{2,o}}$ varies from 1 to $\frac{\gamma_1 - 1}{\gamma_1}$, and $\frac{\Delta M_{2,d}}{M_2}\frac{p_2}{\Delta p_{2,o}}$ varies from 0 to $-\frac{\gamma_1 - 1}{2\gamma_1}$. In interpreting these results, it should be noted that $\Delta p_{2,o}$ and $\Delta u_{2,o}$ are negative. Thus, there is only a slight increase in $\Delta M_{2,d}$, and $\Delta p_{2,d}$ remains essentially constant, during the course of an experiment employing an air-air shock tube at large pressure ratios.

CONCLUDING REMARKS

The calculations which have been made herein are of use in several kinds of shock-tube studies. Probably, the most important application is the prediction of the variation of free-stream conditions at a stationary model (or instrument) utilizing the hot gas region of a shock tube. If the shock tube is to be used for the study of boundary-layer stability or dissociation effects on the development of the boundary layer behind the shock, then the nonuniformities derived herein are also of interest.

The limitations of the present method are the same as those discussed in reference 1. The use of a zero-thickness expansion wave is valid for small pressure ratios but becomes in error for large pressure ratios. However, for very large pressure ratios the contributions of region 3 (to conditions in region 2) are negligible due to the acoustic-impedance mismatch at the contact surface. Hence, it is only for intermediate shock strengths that the use of a zero-thickness expansion wave is likely to introduce errors. The assumption that the boundary layer generates only longitudinal waves introduces a steep gradient of the perturbation quantities directly behind the shock (e.g., fig. 2). (This is due both to the singular nature of the boundary layer and to the assumption of one-dimensional flow within the potential-flow core.) The gradient is steeper for the laminar case (when v_2 has a $\frac{1}{2}$-order singularity directly behind the shock) than for the turbulent case (where v_2 has a $\frac{1}{5}$-order singularity). If the three-dimensional nature of the flow is taken into account, the steep gradient behind the shock would be expected to be somewhat modified. In experimental studies of the relaxation effects associated with strong shocks, it may be necessary to distinguish between the perturbations due to relaxation effects and those due to the wave system introduced by the wall boundary layer.

Lewis Flight Propulsion Laboratory
National Advisory Committee for Aeronautics
Cleveland, Ohio, April 12, 1957

4286

CF-3

APPENDIX A

SYMBOLS

a	speed of sound
C	reflection coefficient at interface, eq. (3)
c_v	specific heat at constant volume
D	transmission coefficient at interface, eq. (3)
d	hydraulic diameter, ft
E	reflection coefficient at shock, eq. (5)
L_2,L_3	eq. (7); ref. 1, appendixes D and E
M	Mach number of flow relative to wall
M_s	Mach number of shock wave relative to wall
n_2,n_3	eq. (7); ref. 1, appendixes D and E
p	pressure
T	temperature, $^{\circ}R$
t	time, sec
u_s	velocity of shock wave relative to wall
u_2	velocity in region 2 relative to wall
v	vertical velocity at edge of boundary layer
x	longitudinal distance from diaphragm
γ	ratio of specific heats
Δ	perturbation from ideal (no attenuation) shock-tube flow
ν	kinematic viscosity
ξ	integration variable representing x
ρ	mass density

τ integration variable representing t

$a,b,\cdots$
$\bar{a},\bar{b},\cdots$ points on characteristic lines (fig. 1); point d is an arbitrary point in region 2

4286

Subscripts:

$a,b,\cdots$
$\bar{a},\bar{b},\cdots$ points in x,t diagram (fig. 1); subscript 2,d refers to arbitrary point in region 2

o condition at shock wave; subscript 2,o refers to conditions in region 2 directly behind shock

w wall

1,2,3,4 regions of shock tube (fig. 1)

Superscripts:

+,- associated with waves moving in + or - x-direction, respectively

Special notation:

$a_{43} \equiv a_4/a_3$; $L_{32} \equiv L_3/L_2$;$\cdots$ two successive integer subscripts, not separated by a comma, represent a ratio

4286

CF-3 back

APPENDIX B

PERTURBATIONS IN REGION 2

Useful expressions relating the perturbation quantities in region 2 are derived herein. The perturbations represent the departure from the ideal conditions that would exist in region 2 if the wall boundary layer were not present. A perfect gas is assumed so that $\gamma_2 = \gamma_1$.

Perturbations Directly Behind Shock

Under ideal conditions, regions 1 and 2 are related by the normal-shock relations

$$\left.\begin{aligned} \frac{p_2}{p_1} &= \frac{2\gamma_1 M_s^2 - (\gamma_1 - 1)}{\gamma_1 + 1} \\ \frac{u_2}{a_1} &= \frac{2}{\gamma_1 + 1}\,\frac{M_s^2 - 1}{M_s} \\ \frac{\rho_2}{\rho_1} &= \frac{(\gamma_1 + 1)M_s^2}{(\gamma_1 - 1)M_s^2 + 2} \end{aligned}\right\} \tag{B1}$$

where M_s is the shock Mach number. If the shock is perturbed, conditions directly behind the shock (designated by subscript 2,o) can be expressed as

$$\left.\begin{aligned}
\frac{\Delta p_{2,o}}{p_2} &= \frac{4\gamma_1 M_s^2}{2\gamma_1 M_s^2 - (\gamma_1 - 1)} \frac{\Delta M_s}{M_s} \\
\frac{\Delta M_s}{M_s} &= \frac{2\gamma_1 M_s - (\gamma_1 - 1)}{4\gamma_1 M_s^2} \frac{\Delta p_{2,o}}{p_2} \\
\frac{\Delta u_{2,o}}{u_2} &= \frac{2\gamma_1 M_s^2 - (\gamma_1 - 1)}{4\gamma_1 M_s^2} \frac{M_s^2 + 1}{M_s^2 - 1} \frac{\Delta p_{2,o}}{p_2} \\
\frac{\Delta \rho_{2,o}}{\rho_2} &= \frac{2\gamma_1 M_s^2 - (\gamma_1 - 1)}{\gamma M_s^2[(\gamma_1 - 1)M_s^2 + 2]} \frac{\Delta p_{2,o}}{p_2} \\
\frac{\Delta T_{2,o}}{T_2} &= \frac{\Delta p_{2,o}}{p_2} - \frac{\Delta \rho_{2,o}}{\rho_2} \text{ (Equation of state)} \\
\frac{\Delta s_{2,o}}{c_v} &= \frac{\Delta p_{2,o}}{p_2} - \gamma \frac{\Delta \rho_{2,o}}{\rho_2} \\
&= \frac{(\gamma_1 - 1)\left(M_s^2 - 1\right)^2}{M_s^2[(\gamma_1 - 1)M_s^2 + 2]} \frac{\Delta p_{2,o}}{p_2}
\end{aligned}\right\} \tag{B2}$$

where $\Delta s_{2,o}$ is the entropy perturbation.

Entropy Variation in Region 2

The entropy is constant for a given particle in region 2, the value depending on the strength of the shock at the instant the particle passed through it. A particle at x,t in region 2 passed through the shock at x_A,t_A where

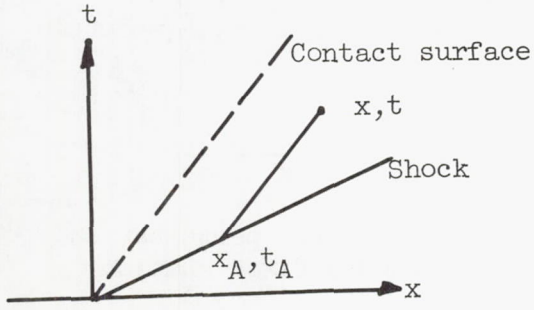

$$\left.\begin{aligned}
\frac{x_A}{x} &= \frac{1 - \frac{u_s t}{x}\frac{u_2}{u_s}}{1 - \frac{u_2}{u_s}} \\
\frac{t_A}{t} &= \frac{\frac{x}{u_s t} - \frac{u_2}{u_s}}{1 - \frac{u_2}{u_s}}
\end{aligned}\right\} \tag{B3}$$

4286

The entropy of a particle at x,t is then given by

$$\frac{\Delta s_{2,d}}{c_v} = \frac{(\gamma_1 - 1)(M_s^2 - 1)^2}{M_s^2[(\gamma_1 - 1)M_s^2 + 2]}\left(\frac{\Delta p_{2,o}}{p_2}\right)_{x_A,t_A} \tag{B4}$$

For weak shocks, equation (B4) is of the order of $(M_s - 1)^3$ and the entropy variations are negligible. The entropy perturbations do not interact with the longitudinal pressure waves, to the order of the present analysis, so that each can be considered separately.

Parametric Form of Perturbation Solutions

For wholly laminar boundary layers $(n = 1/2)$ or wholly turbulent boundary layers $(n = 1/5)$ throughout the shock tube, the local perturbation of any quantity in region 2 (designated by $\Delta(\ )_{2,d}$) can be expressed in the forms

$$\left.\begin{aligned} \frac{\Delta(\ )_{2,d}}{(u_s t)^{1-n}} &= f\left(\frac{x}{u_s t}\right) \\ \frac{\Delta(\ )_{2,d}}{(x)^{1-n}} &= g\left(\frac{x}{u_s t}\right) \end{aligned}\right\} \tag{B5}$$

where $g\left(\frac{x}{u_s t}\right) \equiv \left(\frac{u_s t}{x}\right)^{1-n} f\left(\frac{x}{u_s t}\right)$. The form of equation (B5) can be deduced from equations (9). The function $f\left(\frac{x}{u_s t}\right)$ can be interpreted as the variation with x at a fixed time t while the function $g\left(\frac{x}{u_s t}\right)$ can be interpreted as the variation with t at a fixed x. Both forms are used in figures 2 to 11. When dealing with perturbations normalized to conditions directly behind the shock (i.e., $\Delta(\ )_{2,d}/\Delta(\ )_{2,o}$), multiplication by $(u_s t/x)^{1-n}$ converts a solution for fixed t to a solution for fixed x.

Perturbations at Fixed x for Times $1 \leqslant \frac{u_s t}{x} \leqslant \frac{u_s}{u_2}$

Let subscript $2,o$ be considered to represent the perturbation directly behind the shock at the instant it passes a fixed station x

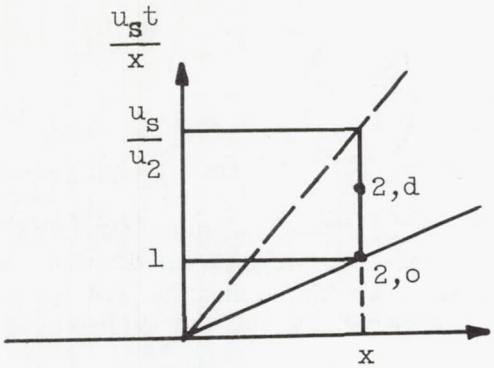

and let subscript 2,d represent the perturbation at the station at a subsequent time. Conditions directly behind the shock can be found by (a) experimental determination of ΔM_s or $\Delta p_{2,o}/p_2$ and equation (B2) or (b) analytical determination of $\Delta p_{2,o}/p_2$ from equations (9) (or fig. 4 for an air-air shock tube) and (B2). The subsequent perturbations can then be expressed as indicated in the following section.

The entropy perturbation may be written in the form

$$\frac{\Delta s_{2,d}}{c_v}\frac{p_2}{\Delta p_{2,o}} = \frac{(\gamma_1 - 1)(M_s^2 - 1)^2}{M_s^2[(\gamma_1 - 1)M_s^2 + 2]}\left(\frac{1 - \frac{u_s t}{x}\frac{u_2}{u_s}}{1 - \frac{u_2}{u_s}}\right)^{1-n} \tag{B6}$$

which is obtained from equations (B4), (B5), and (B3) by noting

$$\frac{(\Delta p_{2,o})_{x_A,t_A}}{\Delta p_{2,o}} = \left(\frac{x_A}{x}\right)^{1-n} = \left(\frac{1 - \frac{u_s t}{x}\frac{u_2}{u_s}}{1 - \frac{u_2}{u_s}}\right)^{1-n}$$

Other perturbations of interest are

$$\frac{\Delta\rho_{2,d}}{\rho_2}\frac{p_2}{\Delta p_{2,o}} = \frac{1}{\gamma}\left(\frac{\Delta p_{2,d}}{\Delta p_{2,o}} - \frac{\Delta s_{2,d}}{c_v}\frac{p_2}{\Delta p_{2,o}}\right) \tag{B7a}$$

$$\frac{\Delta T_{2,d}}{T_2}\frac{p_2}{\Delta p_{2,o}} = \frac{\gamma_1 - 1}{\gamma_1}\frac{\Delta p_{2,d}}{\Delta p_{2,o}} + \frac{1}{\gamma_1}\frac{\Delta s_{2,d}}{c_v}\frac{p_2}{\Delta p_{2,o}} \tag{B7b}$$

$$\frac{\Delta M_{2,d}}{M_2}\frac{p_2}{\Delta p_{2,o}} = \left(\frac{\Delta u_{2,o}}{u_2}\frac{p_2}{\Delta p_{2,o}}\right)\frac{\Delta u_{2,d}}{\Delta u_{2,o}} - \frac{1}{2}\left(\frac{\Delta T_{2,d}}{T_2}\frac{p_2}{\Delta p_{2,o}}\right) \tag{B7c}$$

$$\frac{\Delta q_{2,d}}{q_2}\frac{p_2}{\Delta p_{2,o}} = \frac{\Delta\rho_{2,d}}{\rho_2}\frac{p_2}{\Delta p_{2,o}} + 2\left(\frac{\Delta u_{2,o}}{u_2}\frac{p_2}{\Delta p_{2,o}}\right)\frac{\Delta u_{2,d}}{\Delta u_{2,o}} \tag{B7d}$$

where $M_2 \equiv u_2/a_2$ and $q_2 \equiv \rho_2 u_2^2/2$. The ratios $\Delta p_{2,d}/\Delta p_{2,o}$ and $\Delta u_{2,d}/\Delta u_{2,o}$ are found from equations (9) and (10) or from figures such as 5 and 6. The ratio $\frac{\Delta u_{2,o}}{u_2}\frac{p_2}{\Delta p_{2,o}}$ can be found from equation (B2).

It is of interest to investigate the nature of the perturbations for very strong shocks. Assuming $M_s^2 \gg 1$ and $\frac{(\gamma_1 - 1)M_s^2}{2} \gg 1$, equations (B2) show

$$\left.\begin{aligned} 2\frac{\Delta u_{2,o}}{u_2}\frac{p_2}{\Delta p_{2,o}} \approx \frac{\Delta T_{2,o}}{T_2}\frac{p_2}{\Delta p_{2,o}} \approx \frac{\Delta s_{2,o}}{c_v}\frac{p_2}{\Delta p_{2,o}} \approx 1 \\ \frac{\Delta\rho_{2,o}}{\rho_2}\frac{p_2}{\Delta p_{2,o}} \approx \frac{\Delta M_{2,o}}{M_2}\frac{p_2}{\Delta p_{2,o}} \approx 0 \end{aligned}\right\} \tag{B8}$$

which defines the perturbations directly behind the shock. The subsequent time variation of the perturbation can then be estimated by considering conditions at the contact surface, $\frac{u_s t}{x} = \frac{u_s}{u_2}$. For an air-air shock tube and $M_s \approx O(6)$, figures 5 and 6 indicate that at the contact surface

$$\left.\begin{aligned} \frac{\Delta u_{2,d}}{\Delta u_{2,o}} \approx 0 \\ \frac{\Delta p_{2,d}}{\Delta p_{2,o}} \approx 1 \end{aligned}\right\} \tag{B9}$$

Equations (B9) probably are applicable for other driver gases provided M_s is sufficiently large (in order to make $\rho_3 a_3/\rho_2 a_2$ large) so that region 3 has only a small effect on region 2. (See section titled Discussion of Results.) By use of equations (B9), the other perturbations at the contact surface are

$$\gamma_1\frac{\Delta\rho_{2,d}}{\rho_2}\frac{p_2}{\Delta p_{2,o}} \approx \frac{\gamma_1}{\gamma_1 - 1}\frac{\Delta T_{2,d}}{T_2}\frac{p_2}{\Delta p_{2,o}} \approx \frac{-2\gamma_1}{\gamma_1 - 1}\frac{\Delta M_{2,d}}{M_2}\frac{p_2}{\Delta p_{2,o}} \approx 1 \tag{B10}$$

Thus, during the time interval between passage of the shock and passage of the contact surface, $\frac{\Delta p_{2,d}}{\Delta p_{2,o}}$ remains at about 1, $\frac{\Delta u_{2,d}}{\Delta u_{2,o}}$ varies from 1 to 0, $\frac{\Delta \rho_{2,d}}{\rho_2}\frac{p_2}{\Delta p_{2,o}}$ varies from 0 to $1/\gamma_1$, $\frac{\Delta T_{2,d}}{T_2}\frac{p_2}{\Delta p_{2,o}}$ varies from 1 to $\frac{\gamma_1 - 1}{\gamma_1}$, and $\frac{\Delta M_{2,d}}{M_2}\frac{p_2}{\Delta p_{2,o}}$ varies from 0 to $-\frac{\gamma_1 - 1}{2\gamma_1}$. In interpreting these results, recall that $\Delta p_{2,o}$ and $\Delta u_{2,o}$ are negative. It is seen that there is only a slight increase in $\Delta M_{2,d}$ during the course of an experiment.

Perturbations at Time t for x in Range $\frac{u_2}{u_s} \leqslant \frac{x}{u_s t} \leqslant 1$

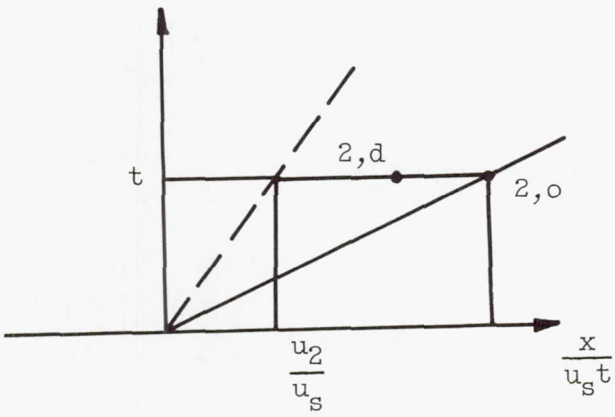

When the variations with x at a fixed time t are considered, subscript 2,o represents conditions directly behind the shock at a fixed time under consideration. The perturbation equations have the same form as in the previous section except for $\Delta s_{2,d}/c_v$, which is now written

$$\frac{\Delta s_{2,d}}{c_v}\frac{p_2}{\Delta p_{2,o}} = \frac{(\gamma_1 - 1)(M_s^2 - 1)^2}{M_s^2[(\gamma_1 - 1)M_s^2 + 2]}\left(\frac{\frac{x}{u_s t} - \frac{u_2}{u_s}}{1 - \frac{u_2}{u_s}}\right)^{1-n} \tag{B11}$$

which follows from

$$\frac{(\Delta p_{2,o})_{x_A,t_A}}{\Delta p_{2,o}} = \left(\frac{t_A}{t}\right)^{1-n} = \left(\frac{\frac{x}{u_s t} - \frac{u_2}{u_s}}{1 - \frac{u_2}{u_s}}\right)^{1-n}$$

This modification is in agreement with the discussion associated with equation (B5), which indicates that a solution for a fixed x can be converted to a solution for a fixed t by multiplying the former by $\left(\frac{x}{u_s t}\right)^{1-n}$.

4286

CF-4

REFERENCES

1. Mirels, Harold: Attenuation in a Shock Tube Due to Unsteady-Boundary-Layer Action. NACA TN 3278, 1956.

2. Trimpi, Robert L., and Cohen, Nathaniel B.: A Theory for Predicting the Flow of Real Gases in Shock Tubes with Experimental Verification. NACA TN 3375, 1955.

3. Williams, Albert Charles: Propagation of the Effects of Wall Interaction in the Rarefaction Region of Shock Tube Flow. Tech. Rep. No. 6, Inst. Res., Lehigh Univ., Aug. 15, 1955. (Proj. NR 061-063, Contract N7onr 39302, Office Naval Res.)

4. Glass, I. I., and Patterson, G. N.: A Theoretical and Experimental Study of Shock-Tube Flows. Jour. Aero. Sci., vol. 22, no. 2, Feb. 1955, pp. 73-100.

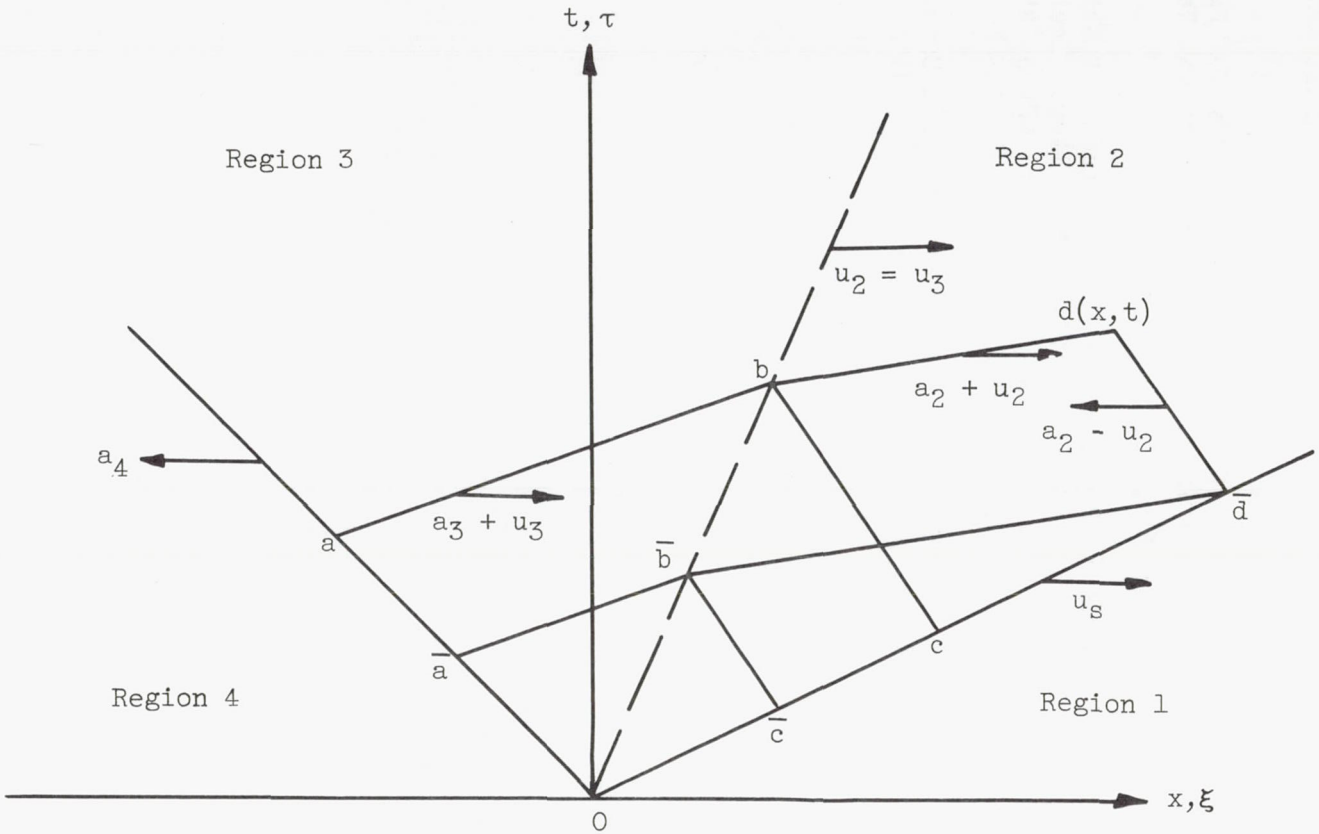

Figure 1. - Characteristic lines contributing to pressure and velocity perturbations at point d(x,t) behind shock.

4286

CF-4 back

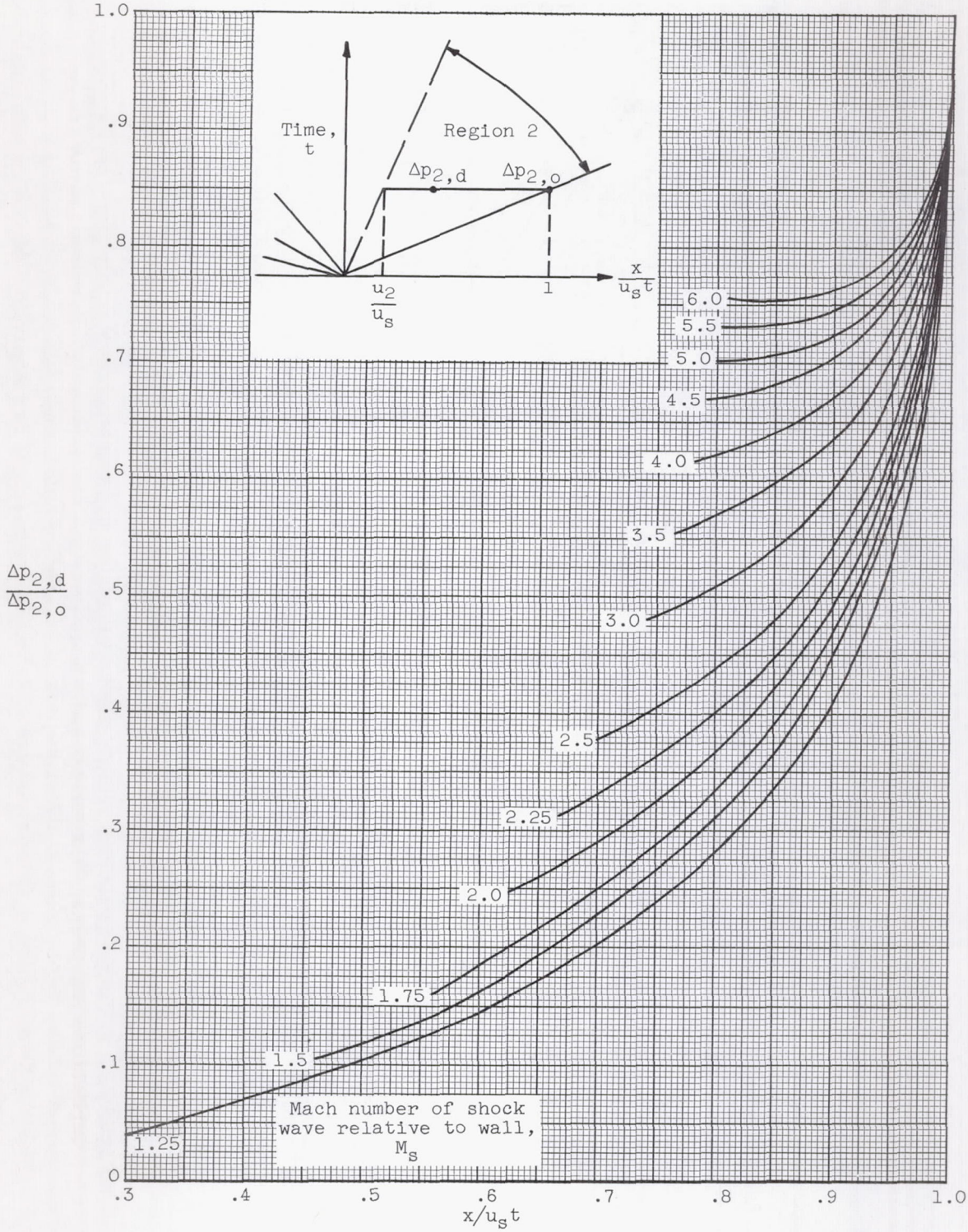

(a) Laminar boundary layer.

Figure 2. - Axial variation of pressure perturbation in region 2 at fixed time. Air-air shock tube, $T_1 = T_4 = T_w = 520^\circ$ R.

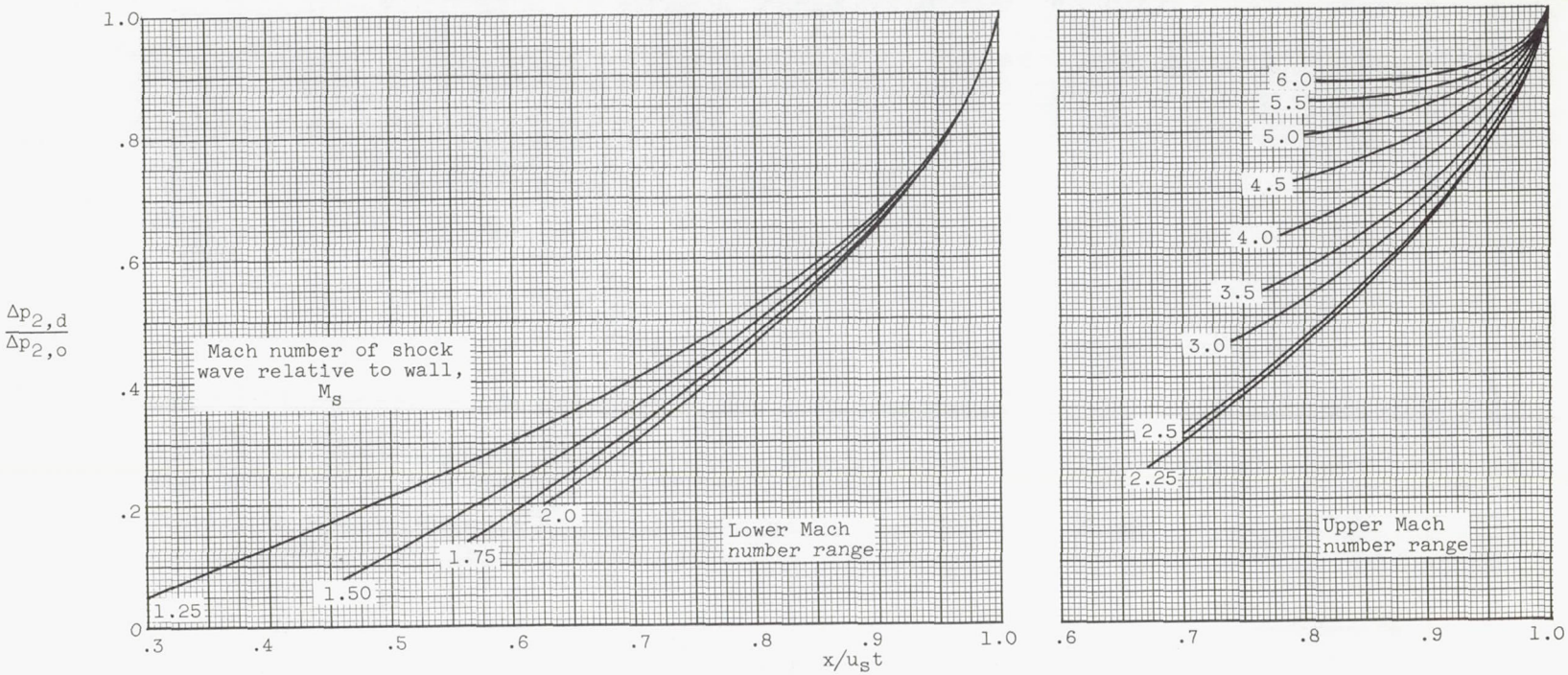

(b) Turbulent boundary layer.

Figure 2. - Concluded. Axial variation of pressure perturbation in region 2 at fixed time. Air-air shock tube, $T_1 = T_4 = T_w = 520^\circ$ R.

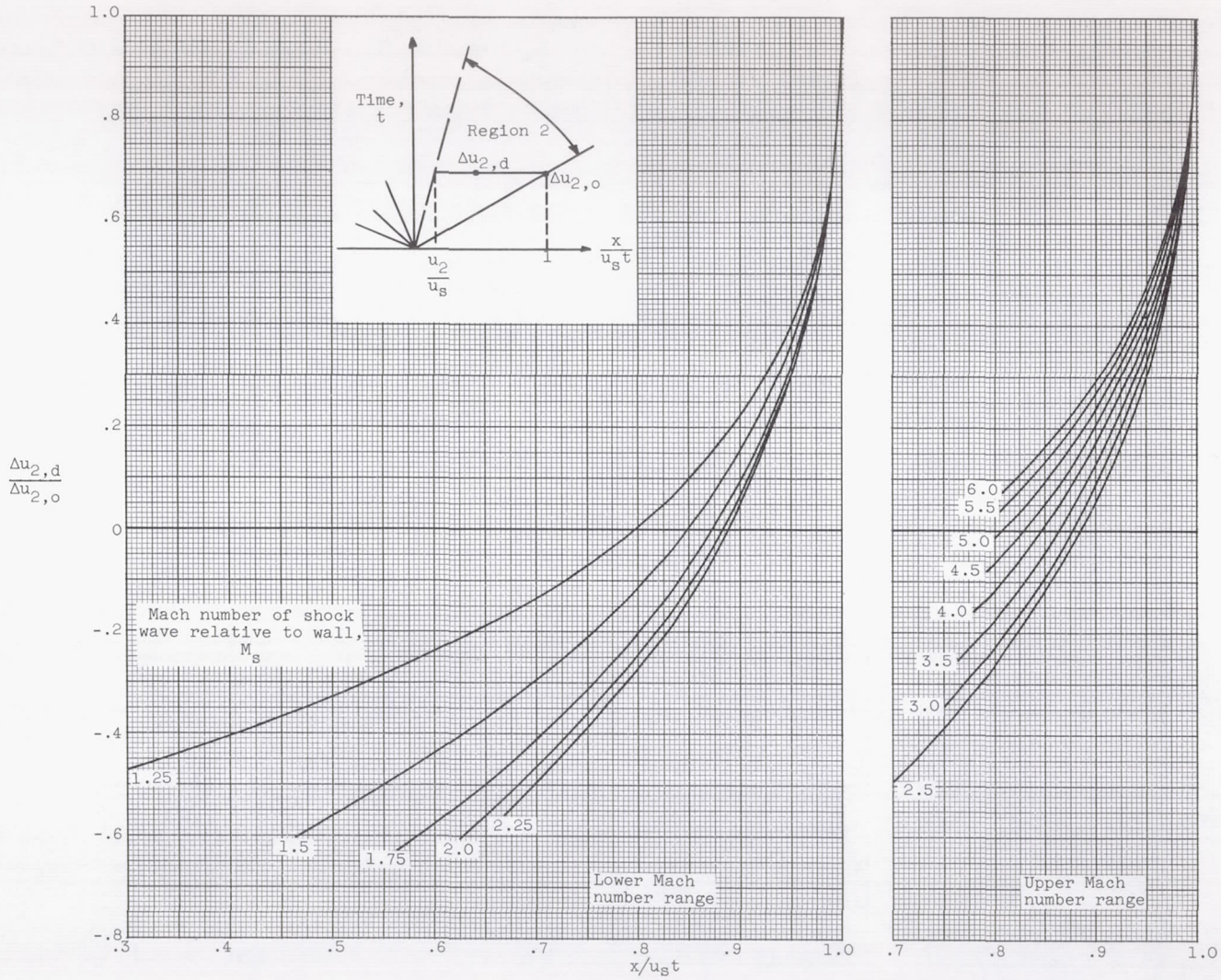

(a) Laminar boundary layer.

Figure 3. - Axial variation of velocity perturbation in region 2 at fixed time. Air-air shock tube, $T_1 = T_4 = T_w = 520^\circ$ R.

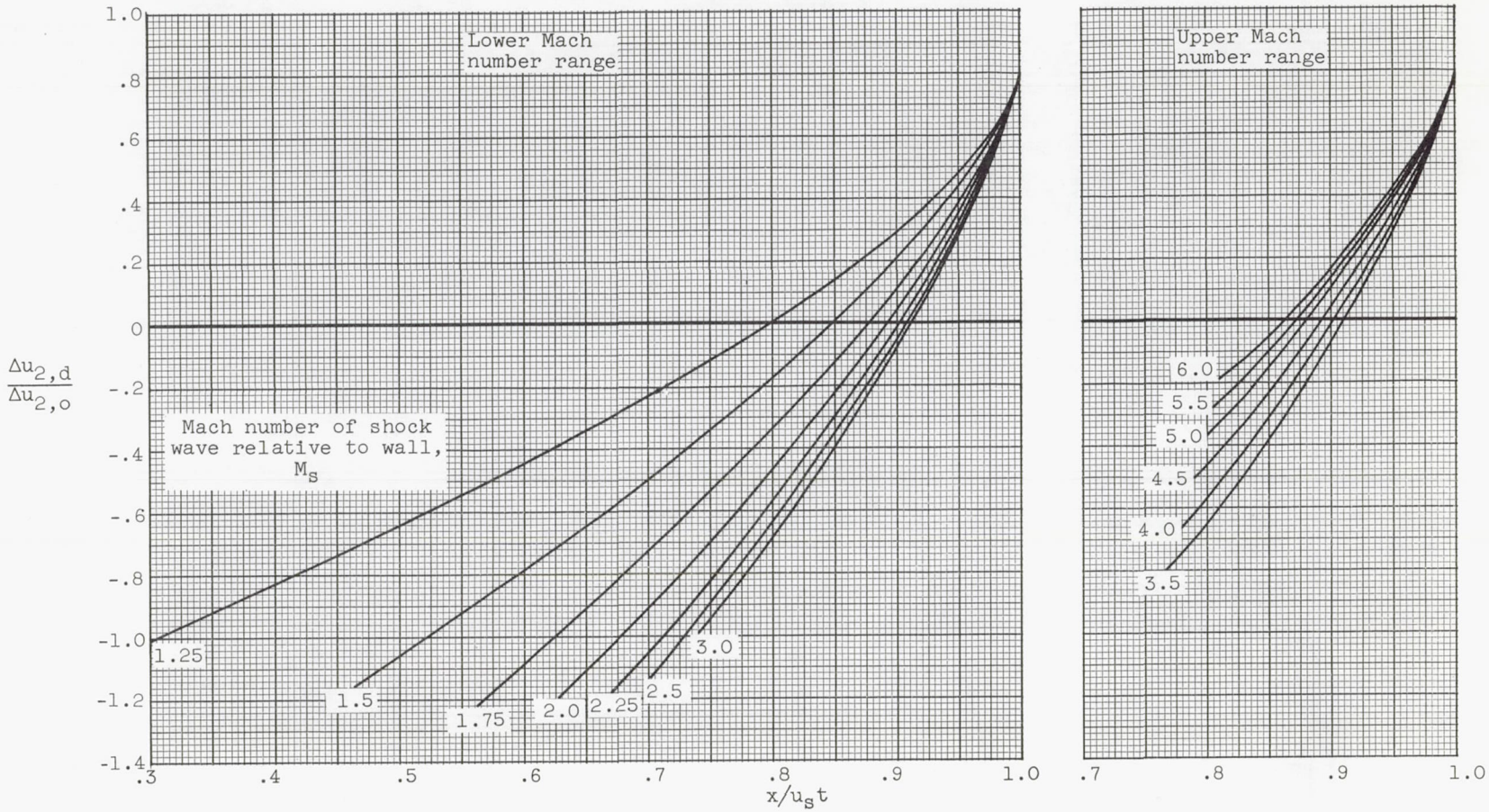

(b) Turbulent boundary layer.

Figure 3. - Concluded. Axial variation of velocity perturbation in region 2 at fixed time. Air-air shock tube, $T_1 = T_4 = T_w = 520^\circ$ R.

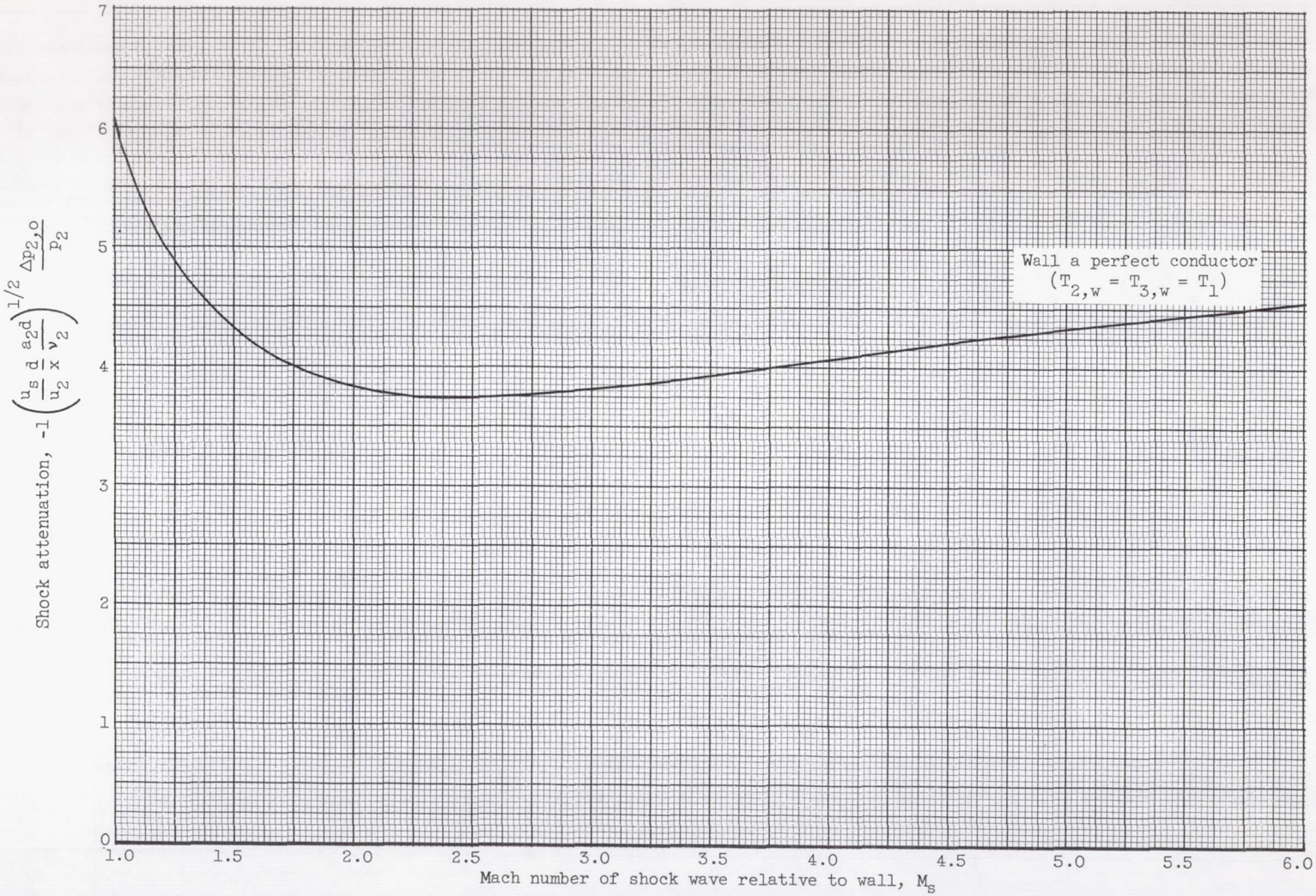

(a) Laminar boundary layer.

Figure 4. - Attenuation in air-air shock tube (ref. 1, fig. 5). $T_1 = T_4 = 520^{\circ}$ R; Prandtl number, 0.70; ratio of specific heats, 1.4.

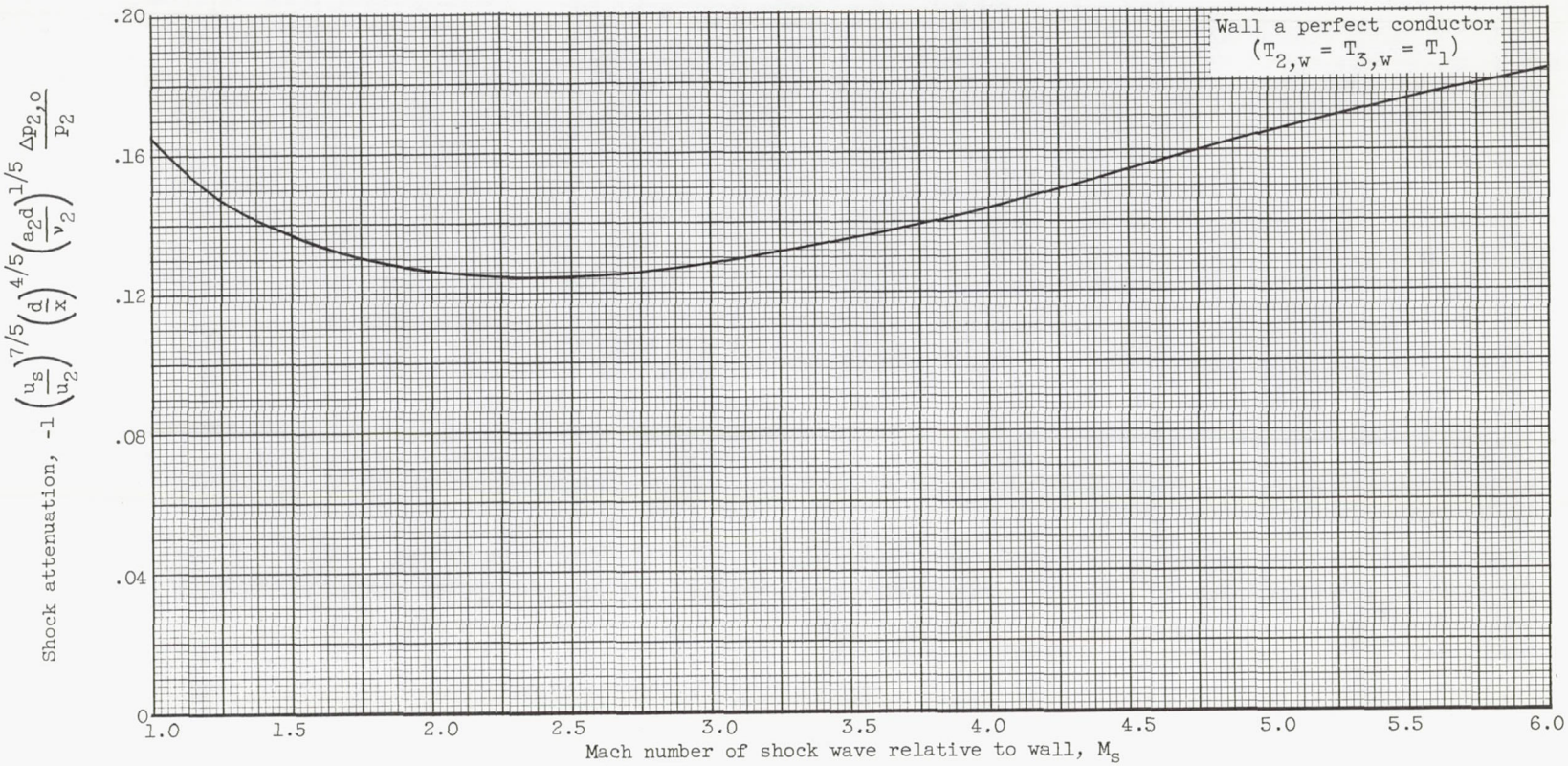

(b) Turbulent boundary layer.

Figure 4. - Concluded. Attenuation in air-air shock tube (ref. 1, fig. 5). $T_1 = T_4 = 520^{\circ}$ R; Prandtl number, 0.70; ratio of specific heats, 1.4.

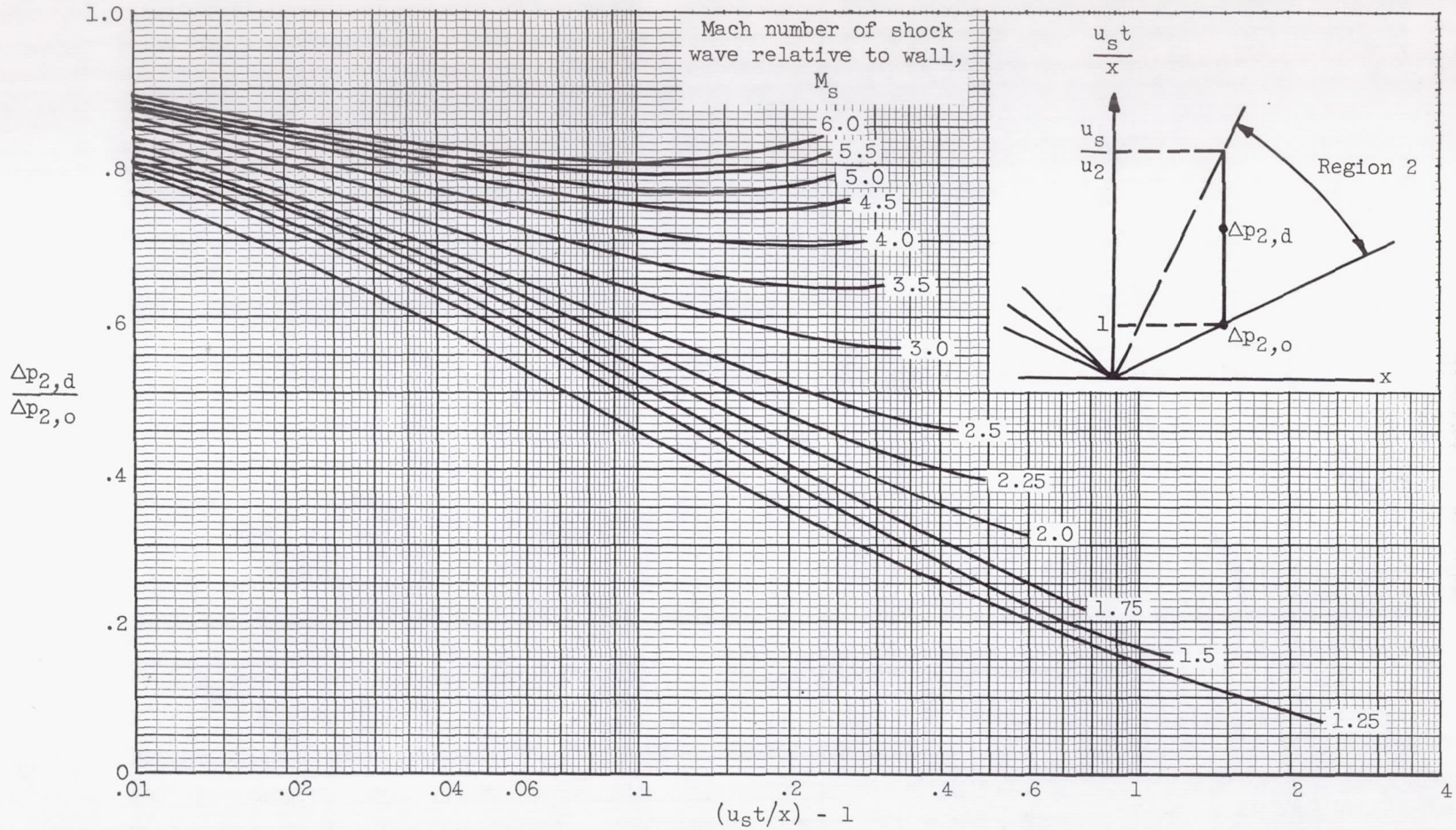

(a) Laminar boundary layer.

Figure 5. - Time variation of pressure perturbation at fixed station x in region 2. Air-air shock tube, $T_1 = T_4 = T_w = 520^\circ$ R.

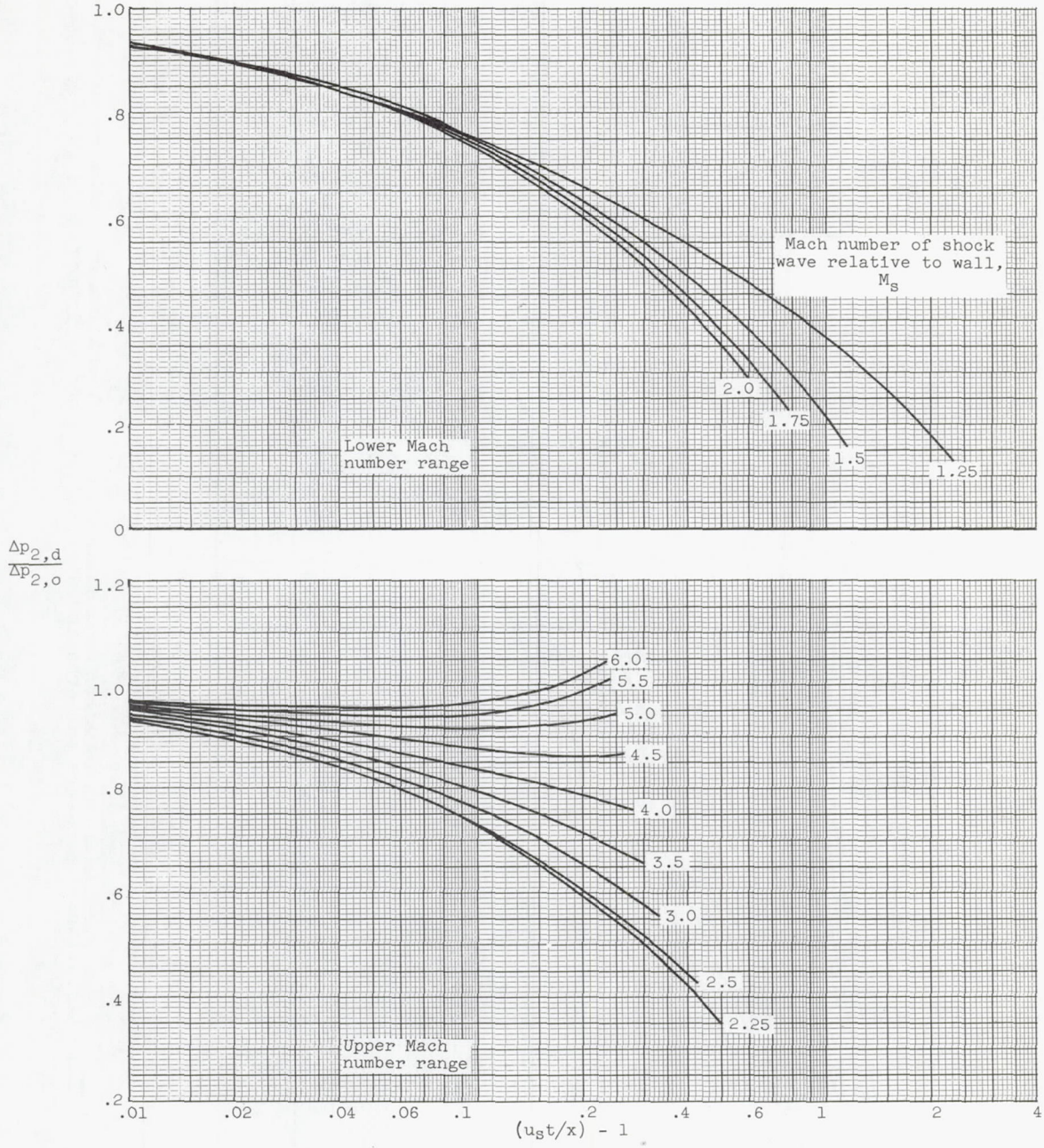

(b) Turbulent boundary layer.

Figure 5. - Concluded. Time variation of pressure perturbation at fixed station x in region 2. Air-air shock tube, $T_1 = T_4 = T_w = 520^\circ$ R.

4286

CF-5 back

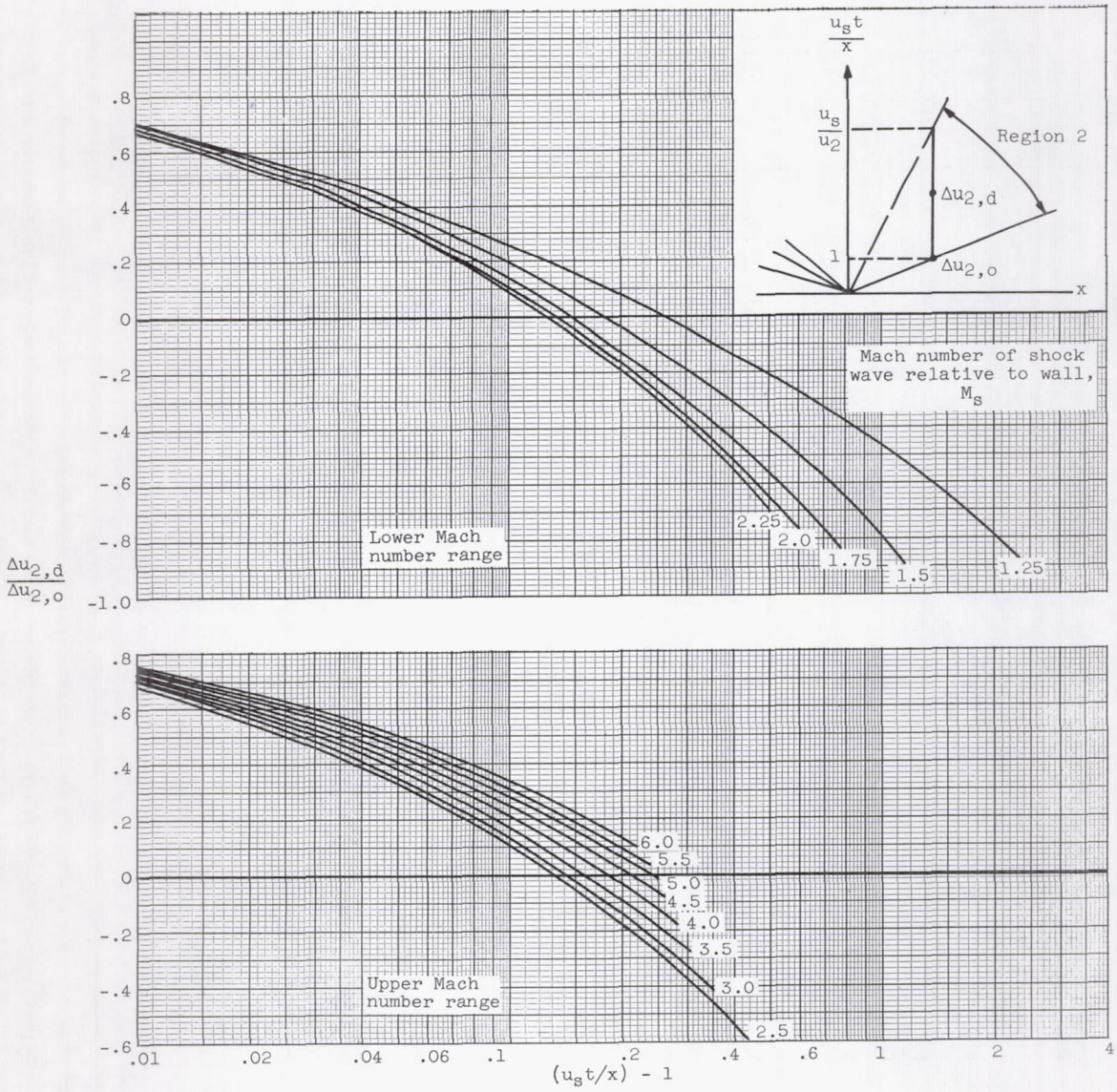

(a) Laminar boundary layer.

Figure 6. - Time variation of velocity perturbation at fixed station x in region 2. Air-air shock tube, $T_1 = T_4 = T_w = 520^\circ$ R.

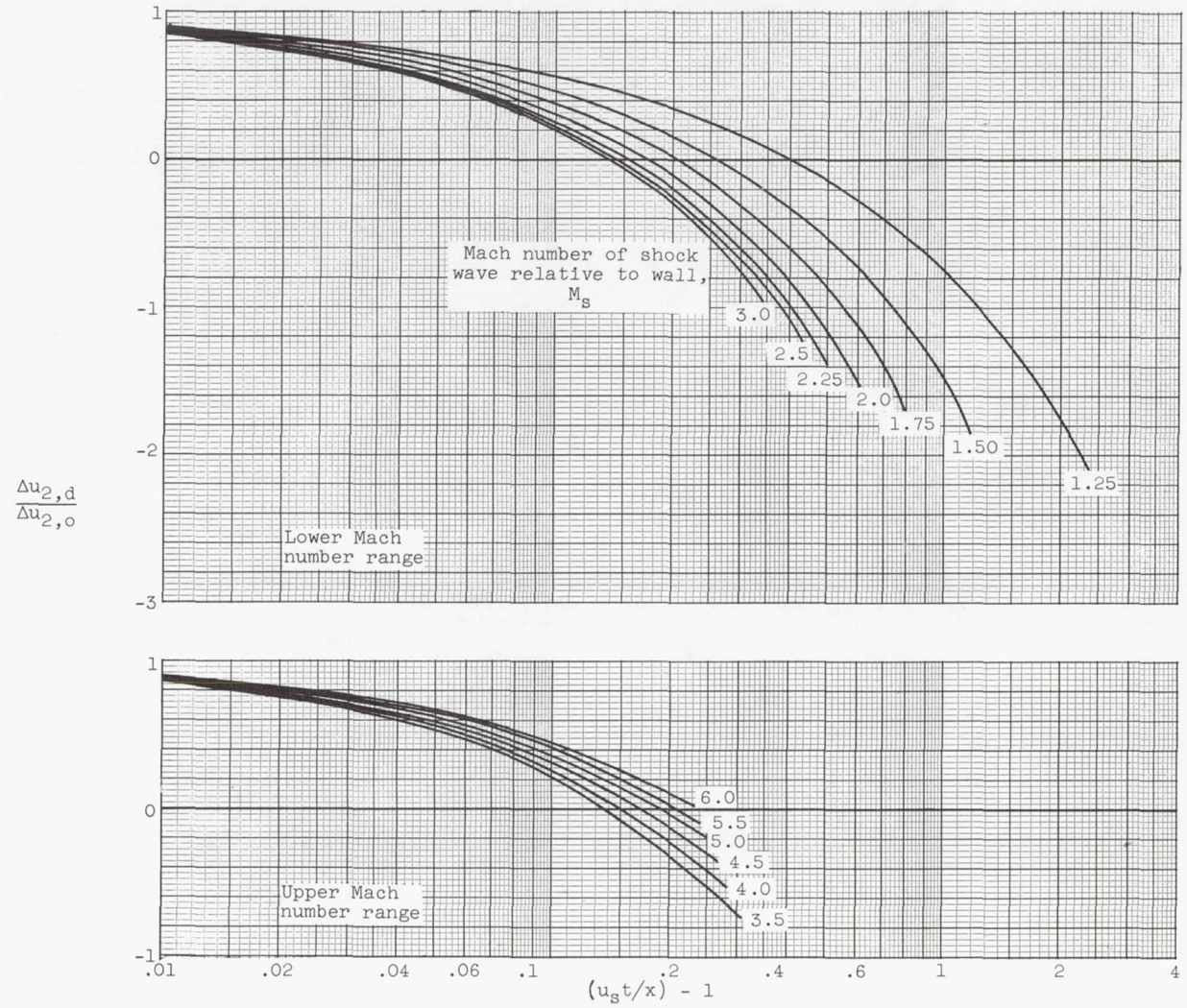

(b) Turbulent boundary layer.

Figure 6. - Concluded. Time variation of velocity perturbation at fixed station x in region 2. Air-air shock tube, $T_1 = T_4 = T_w = 520^\circ$ R.

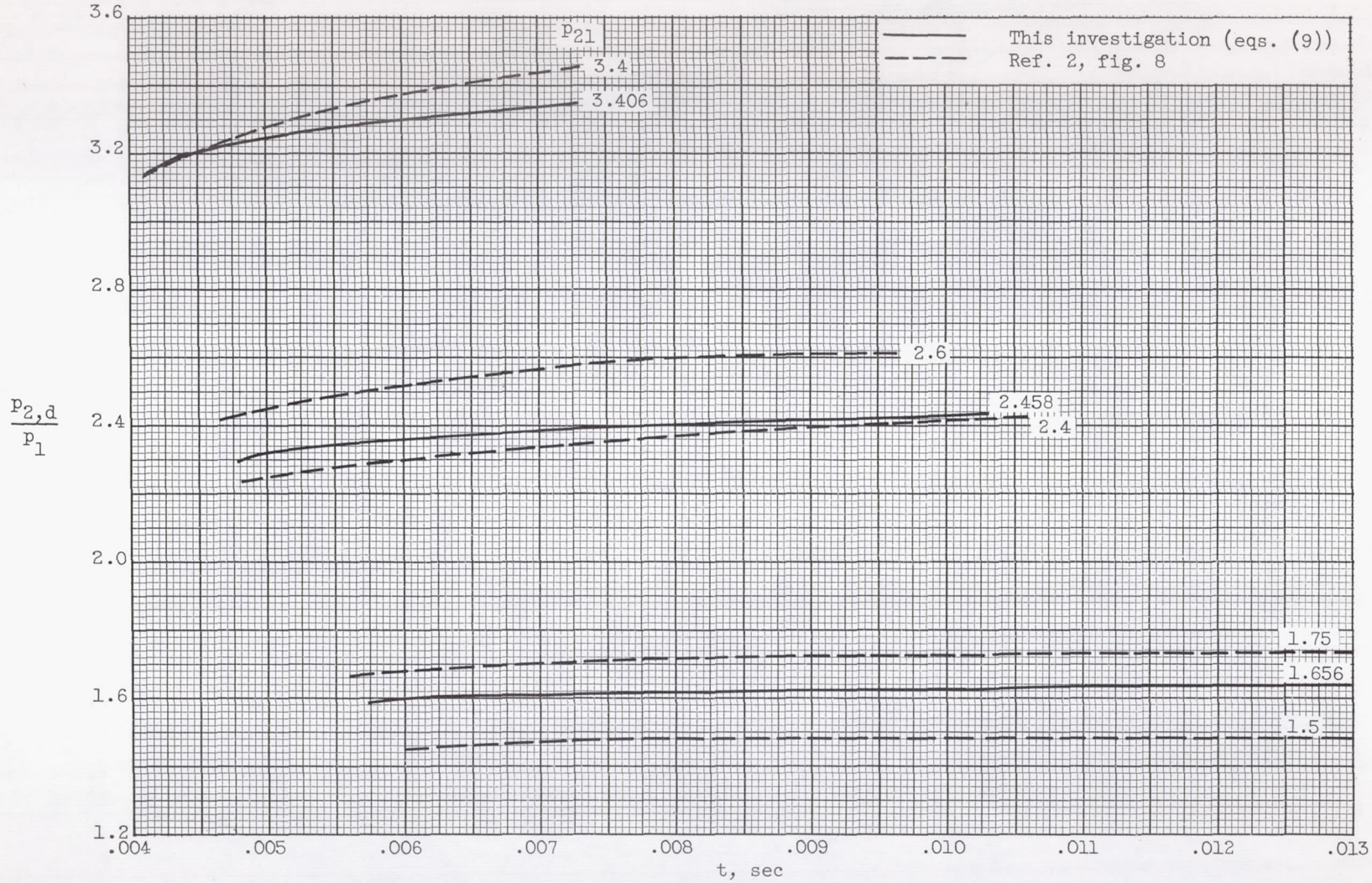

Figure 7. - Time variation of pressure behind shock wave. Turbulent boundary layer; $T_1 = T_4 = T_w = 520^{\circ}$; longitudinal distance from diaphragm, 8 feet; hydraulic diameter, 1/7 foot.

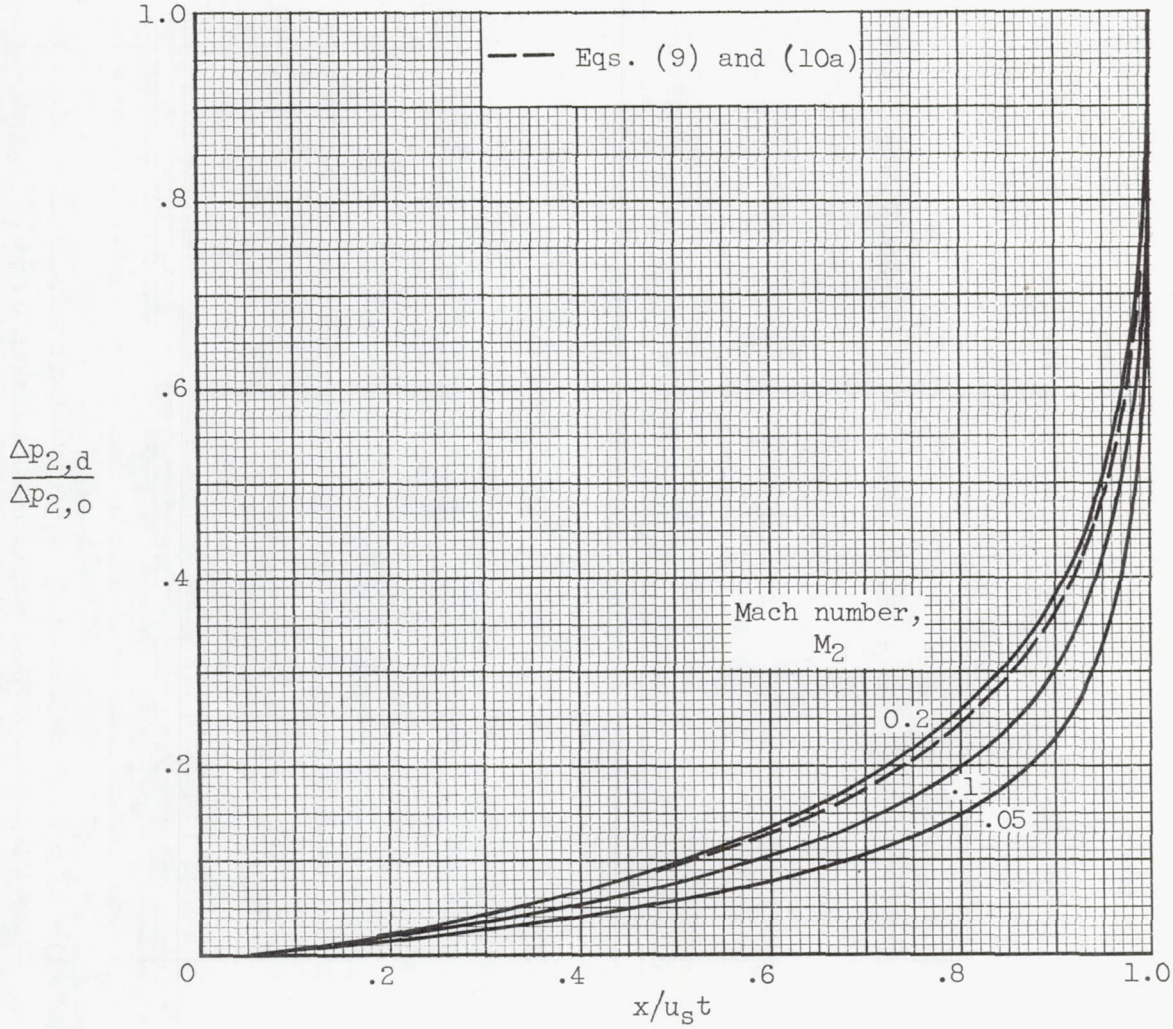

(a) Laminar boundary layer.

Figure 8. - Pressure perturbations (at fixed instant of time) behind weak waves (eq. 12(a)). $\gamma_1 = \gamma_4 = 1.4$; $T_1 = T_4$.

4286

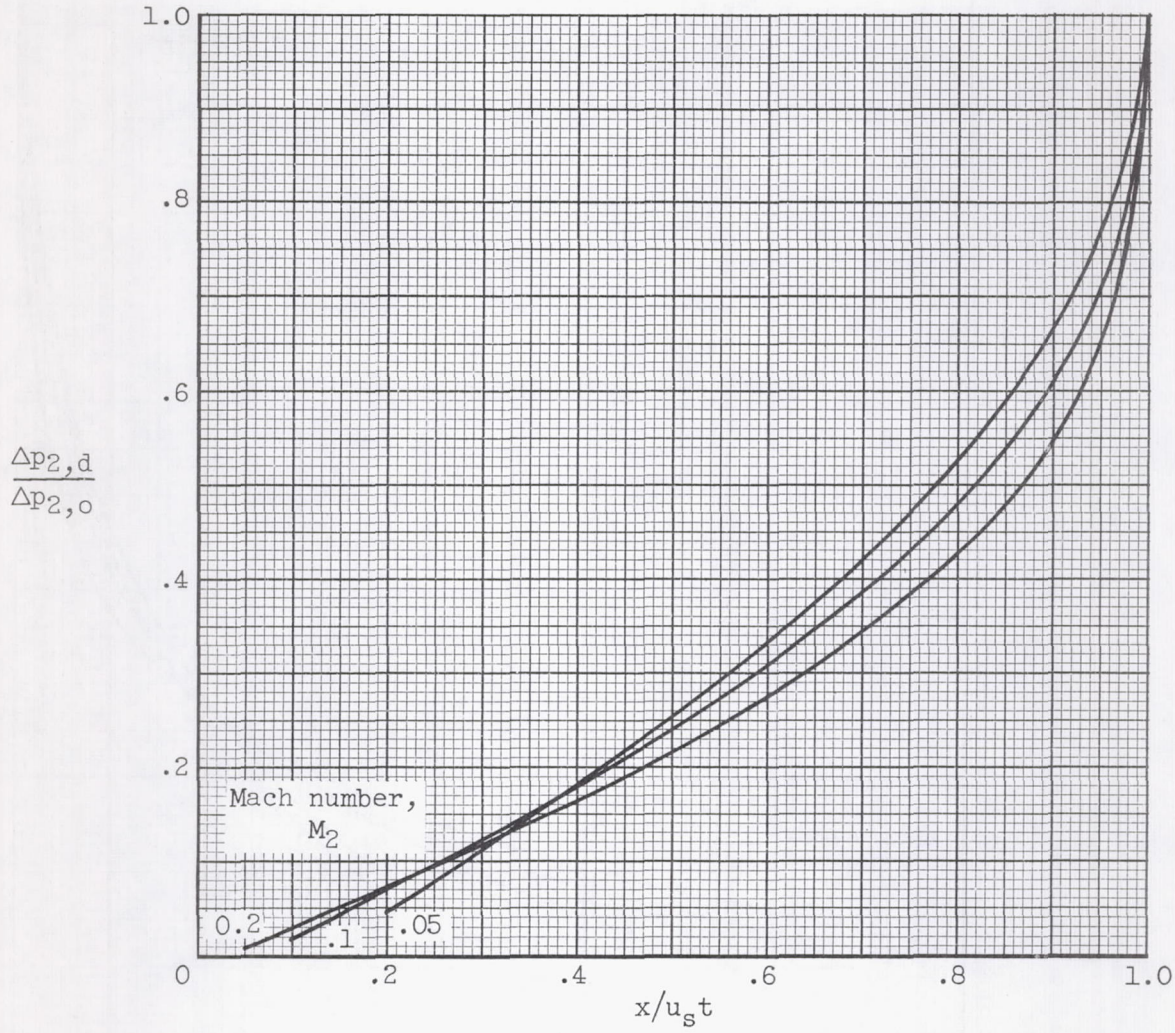

(b) Turbulent boundary layer.

Figure 8. - Concluded. Pressure perturbations (at fixed instant of time) behind weak waves (eq. 12(a)). $\gamma_1 = \gamma_4 = 1.4$; $T_1 = T_4$.

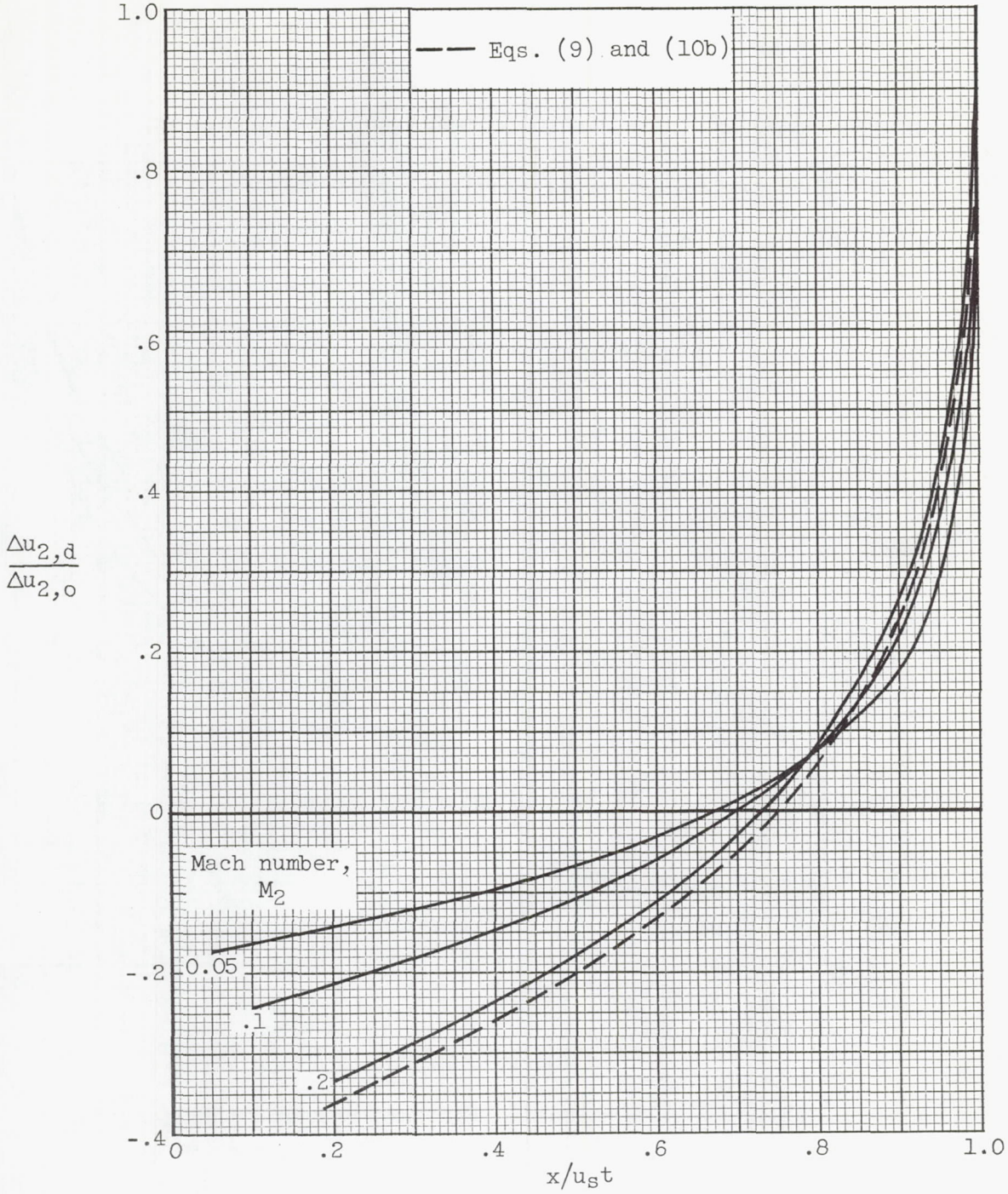

(a) Laminar boundary layer.

Figure 9. - Velocity perturbations (at fixed instant of time) behind weak waves (eq. 12(b)). $\gamma_1 = \gamma_4 = 1.4$; $T_1 = T_4$.

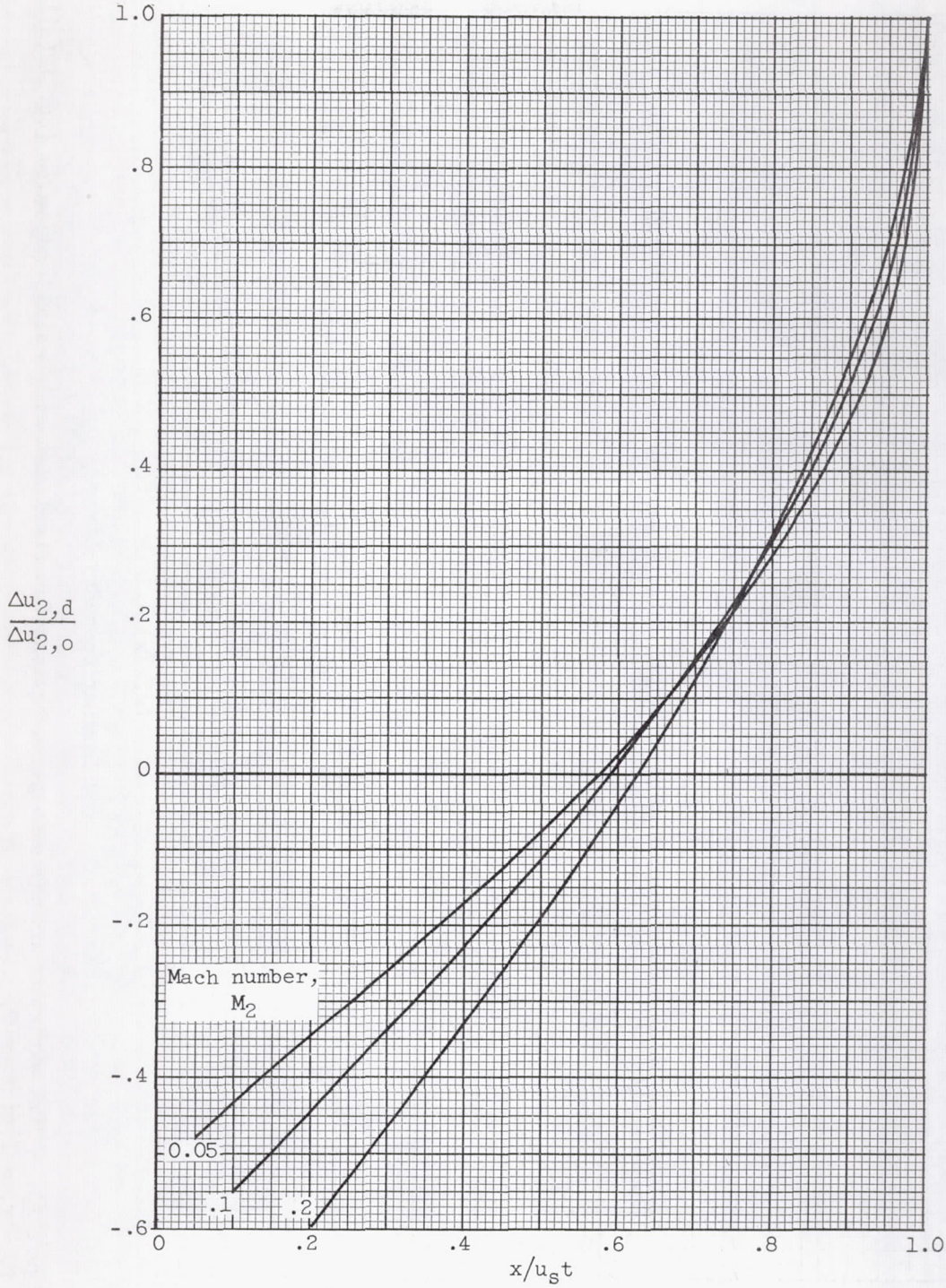

(b) Turbulent boundary layer.

Figure 9. - Concluded. Velocity perturbations (at fixed instant of time) behind weak waves (eq. 12(b)). $\gamma_1 = \gamma_4 = 1.4$; $T_1 = T_4$.

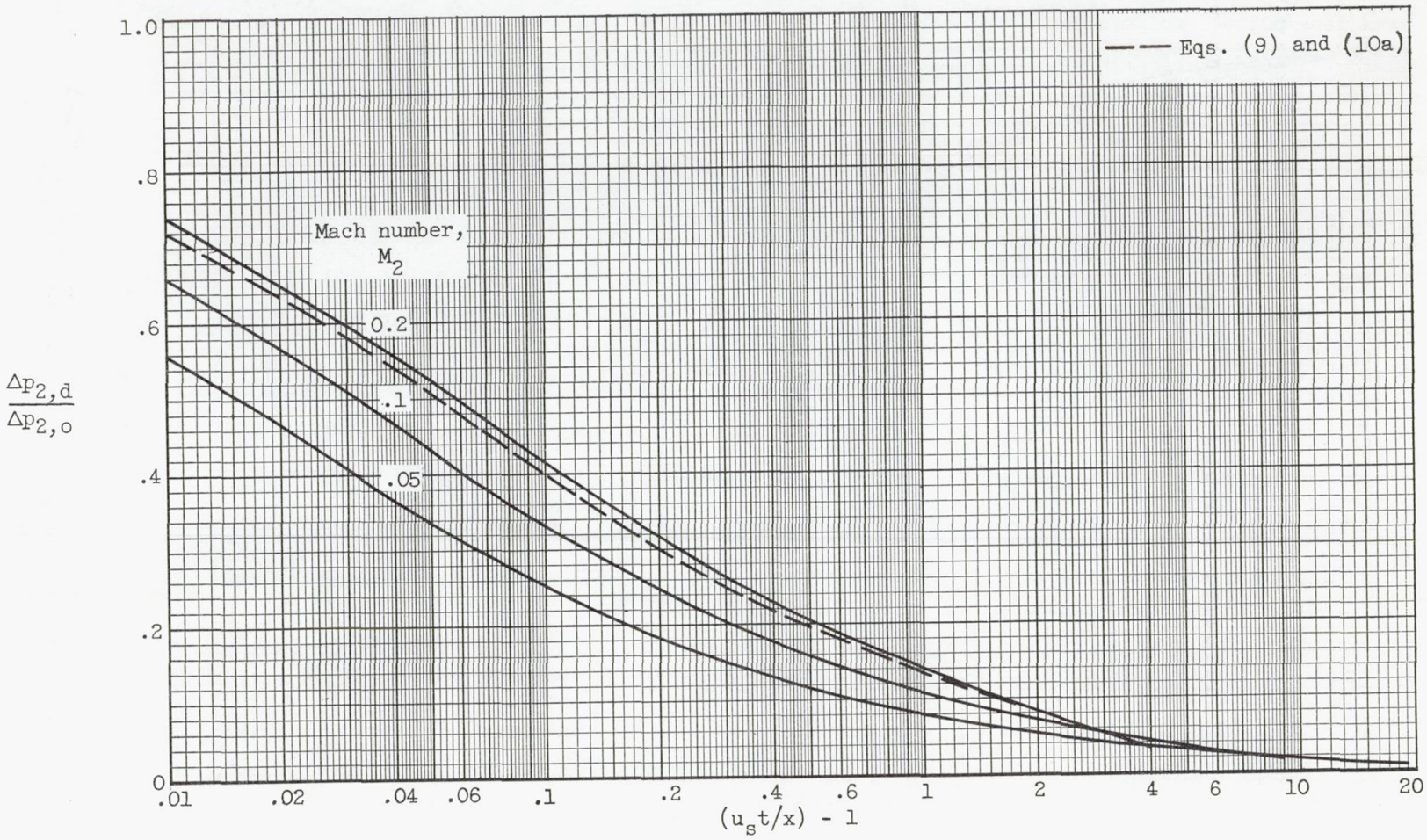

(a) Laminar boundary layer.

Figure 10. - Time variation of pressure perturbations (at fixed station) behind weak waves (eq. 12(a)). $\gamma_1 = \gamma_4 = 1.4$; $T_1 = T_4$.

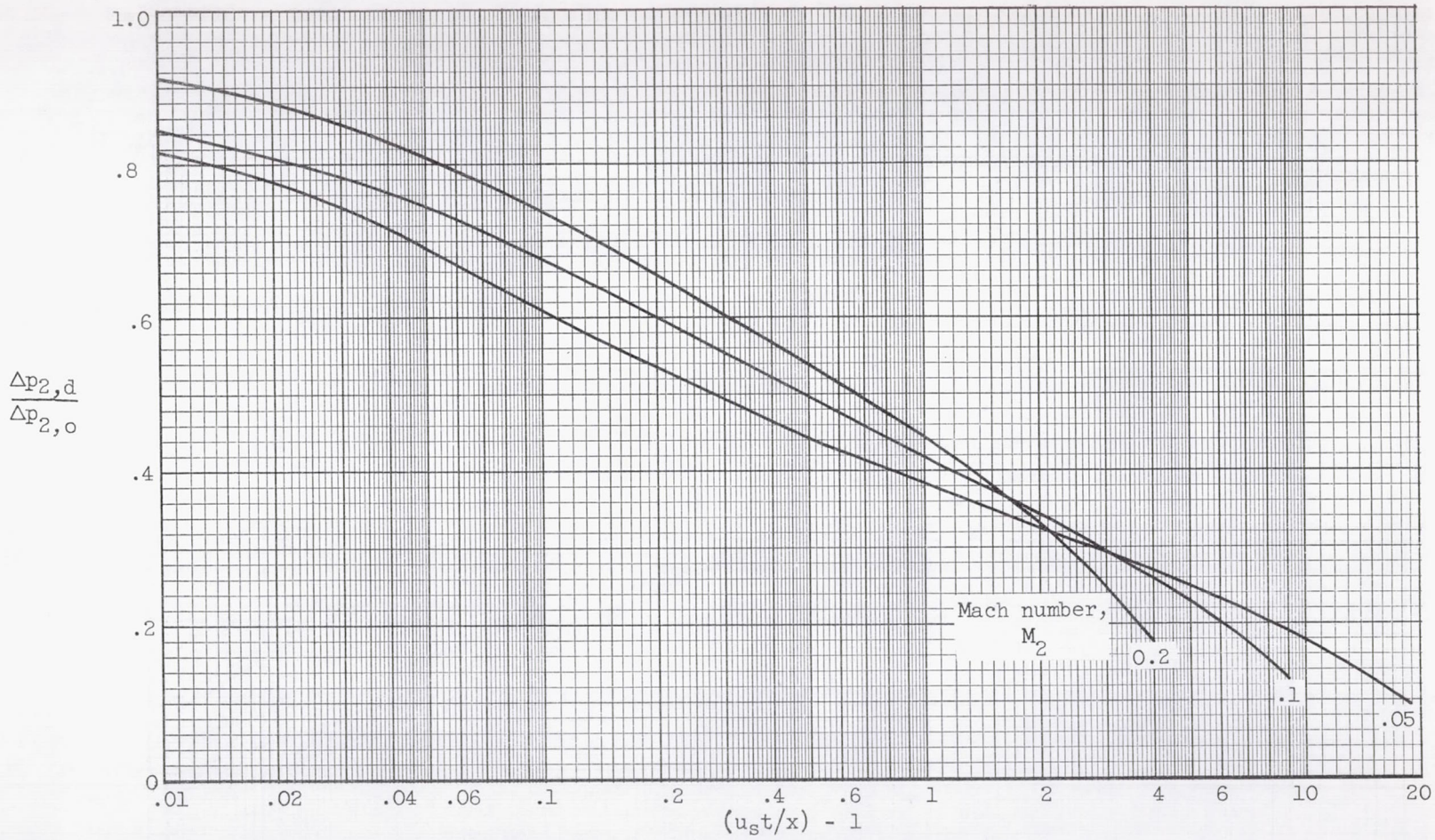

(b) Turbulent boundary layer.

Figure 10 - Concluded. Time variation of pressure perturbations (at fixed station) behind weak waves (eq. 12(a)). $\gamma_1 = \gamma_4 = 1.4$; $T_1 = T_4$.

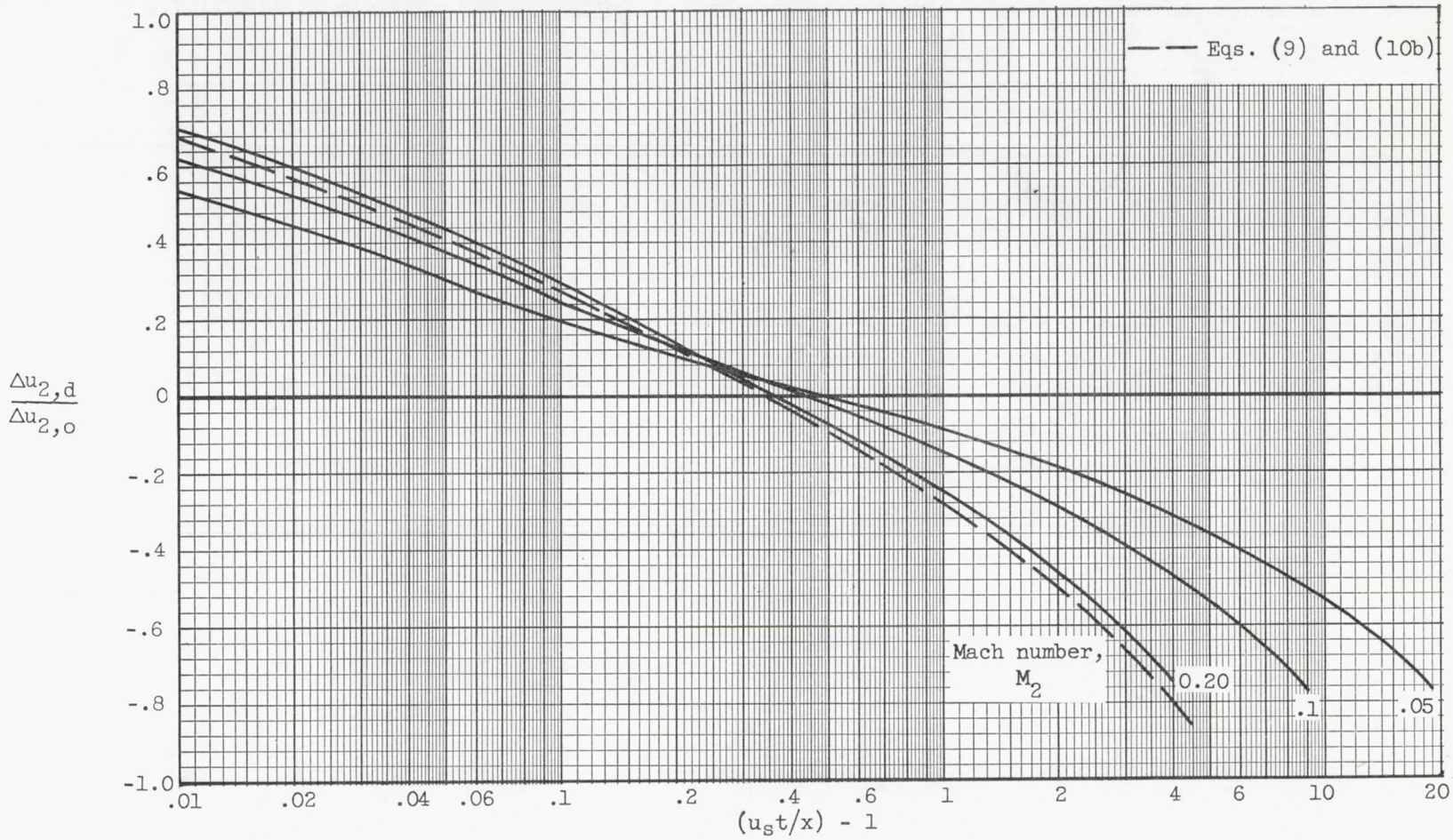

(a) Laminar boundary layer.

Figure 11. - Time variation of velocity perturbations (at fixed station) behind weak waves (eq. 12(b)). $\gamma_1 = \gamma_4 = 1.4$; $T_1 = T_4$.

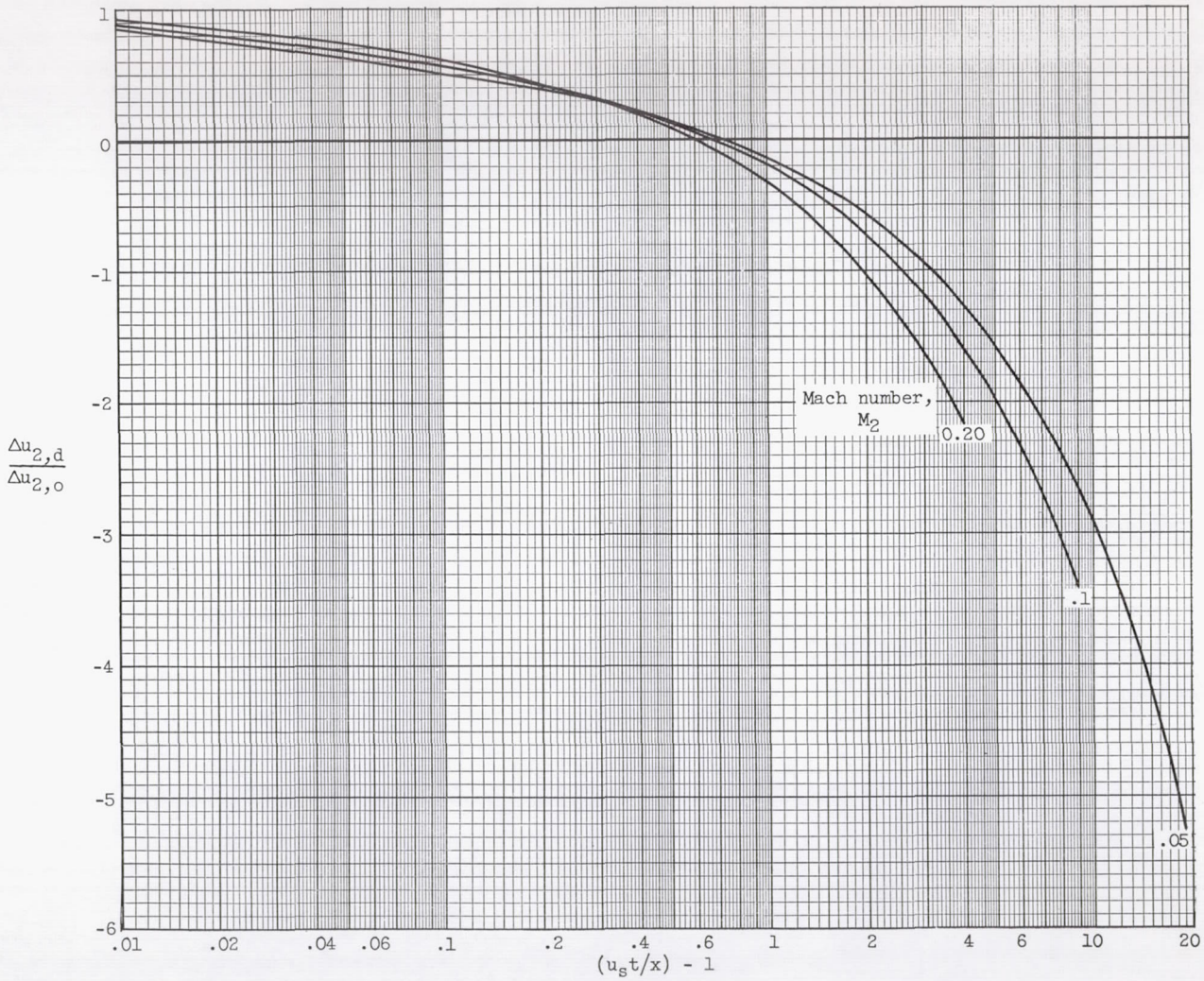

(b) Turbulent boundary layer.

Figure 11. - Concluded. Time variation of velocity perturbations (at fixed station) behind weak waves (eq. 12(b)). $\gamma_1 = \gamma_4 = 1.4$; $T_1 = T_4$.

NACA - Langley Field, Va.